CDF note 8016, v2.2

Search for Heavy, Neutral, Long-Lived Particles that Decay to Photons

Max Goncharov, Vyacheslav Krutelyov*, Eunsin Lee, David Toback, and Peter Wagner
Texas A&M University
(Dated: December 8, 2006)

We present the results of a search for heavy, neutral, long-lived particles that decay to photons in a sample of $\gamma + \not\!\!E_T + \geq 1$ jet events. Candidate events are selected based on the delayed arrival time of the photon at the calorimeter as measured with the EMTiming system. We find 2 events using 570 pb^{-1} of data in run II which is consistent with the background estimate of 1.3±0.7 events. Using a gauge mediated supersymmetry breaking model with $\widetilde{\chi}_1^0 \rightarrow \gamma \widetilde{G}$ we set quasi model-independent cross section limits, as well as find the exclusion region in the $\widetilde{\chi}_1^0$ lifetime vs. mass plane with a mass reach of 101 GeV/c^2 at $\tau_{\tilde{\chi}} = 5$ ns. Our results extend the sensitivity beyond those from LEP II.

* now at University of California, Santa Barbara

Contents

I. INTRODUCTION

We present a search for heavy, neutral, long-lived particles that decay to photons via the signature of a photon with a delayed arrival time, using the EMTiming system [1, 2], at least one jet, and missing transverse energy ($\not\!\!E_T$) at CDF. An example of a theory that would produce these particles is gauge mediated supersymmetry breaking (GMSB) [3], with the lightest neutralino, $\widetilde{\chi}_1^0$, as the next-to-lightest supersymmetric particle (NLSP) and a gravitino, $\widetilde{G}$, as the LSP. This model gained favor with the appearance of the $ee\gamma\gamma\not\!\!E_T$ candidate event in run I [4]. While we use a quasi model-independent approach in our search, we use this model as a benchmark to compare our sensitivity with other searches at LEP [5]. This analysis follows the prescription in Ref. [6] for neutralinos with long lifetimes.

While this is well motivated theoretically and experimentally it would not have been possible without a timing system in the calorimeter. In many ways the timing system in the electromagnetic (EM) calorimeter ("EMTiming") [2] was built in response to the $ee\gamma\gamma\not\!\!E_T$ event, in particular to verify that all EM clusters in future events were from the primary collision; one of the photons and the plug electron in this event had no arrival time information. Because of this ambiguity, the EMTiming system would resolve the problem of determining if the event were from cosmic ray or other non-collision sources (although background estimates of this type are at the 10^{-9} level), or perhaps were the decay product of a long-lived particle that decayed to a photon and/or electron. The system was installed and commissioned in Fall 2004. It covers the central and plug region of the calorimeter up to a pseudo-rapidity (η) of 2.1 with a threshold of ∼3-4 GeV tower energy [1]. With this tool in hand it became feasible to search for events that contain photons with arrival times delayed compared to a prompt production from the collision which allows separation from Standard Model (SM) and non-collision backgrounds.

Theoretically, mainly GMSB models predict long-lived, heavy, neutral particles in the form of $\widetilde{\chi}_1^0$'s with a mass of ∼100 GeV and a lifetime on the order of nanoseconds that decay to photons. At the Tevatron gaugino pair-production and decay produces $\widetilde{\chi}_1^0$'s in association with jets, each $\widetilde{\chi}_1^0$ decaying into a $\widetilde{G}$, that gives rise to $\not\!\!E_T$, and a photon. Depending on how many of the two $\widetilde{\chi}_1^0$'s decay inside the detector, due to their large decay length, the event has the signature $\gamma\gamma + \not\!\!E_T$ or $\gamma + \not\!\!E_T$ with one or more additional jets. Figure 1 illustrates the decay of a $\widetilde{\chi}_1^0$ into a photon and a $\widetilde{G}$. The $\widetilde{\chi}_1^0$ emanates a $\widetilde{G}$, that leaves undetected, and a photon after a macroscopic (∼ns) decay time. Its arrival time at the calorimeter is delayed compared to a prompt photon that would propagate directly from the collision to the same position at the calorimeter. It is these time-delayed photons that we select as the signal region in this analysis.

In this analysis we will focus on the $\gamma + \not\!\!E_T$ case which is more sensitive to higher lifetimes [6].

We perform a blind analysis in the sense that we blind the signal region and select the final event requirements based on the signal and background expectations alone. The background rates are estimated from the photon timing using known background shapes in control regions from the same $\gamma + \not\!\!E_T + \geq 1$ jet dataset. We use GMSB models and a detector simulation to estimate the signal expectations. Before unblinding the signal region we find our final event requirements by optimizing our sensitivity for the lowest expected 95% C.L. expected cross section limits in the $\widetilde{\chi}_1^0$ mass and lifetime region that we are sensitive to. Our search is quasi model-independent in the sense that none of our event requirements makes use of event properties that are manifestly GMSB specific.

We present both model-independent cross section limits as well as exclusion regions in the GMSB parameter space. Our model-independent results parameterize the kinematic and timing acceptance and efficiency as a function of $\widetilde{\chi}_1^0$ mass and lifetime. This parameterization allows for cross section limits that can be used to compare to production cross sections for any model that predicts long- lived, heavy, neutral particles, that decay via our $\gamma + \not\!\!E_T$ event selection criteria. For simplicity, we choose the same GMSB parameter space as used in other analyses, in particular those from ALEPH/LEP [5, 7]. The ALEPH exclusion region results are shown in Fig. 2.

The structure of this note is as follows: Section II explains the GMSB models in more detail. Section III describes the search strategy, the dataset and the baseline event selection. Section IV outlines the different backgrounds and how we estimate them for use in the optimization procedure. Section V describes the Monte Carlo (MC) that we use to model the signal acceptance and Section VI gives the systematic uncertainties on the acceptance and the production cross sections. The optimization procedure, and its result, are shown in Sec. VII. We unblind the signal region in Sec. VIII and compare the observed and expected exclusion regions. We conclude in Sec. IX. This note is designed to be the summary of this search analysis and should be read in conjunction with the supporting material that can be found in the notes in Refs. [1, 9–13]. While we have attempted to summarize the material there, in general the reader is assumed to be familiar with that work. This note is an updated version from the blessing of June 2006 [8].

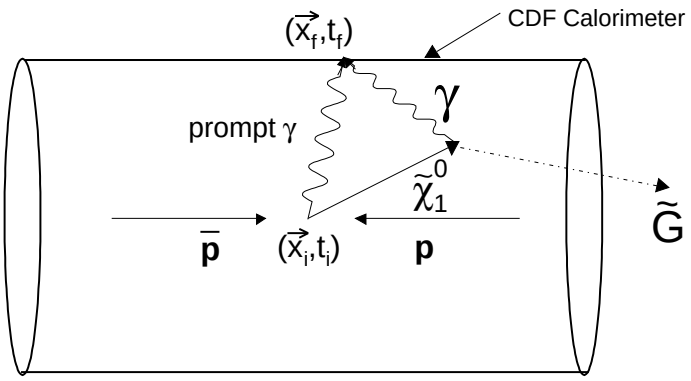

FIG. 1: The schematics of the GMSB process of a long-lived $\widetilde{\chi}_1^0$ decaying into a $\widetilde{G}$ and a photon inside the CDF detector. While the $\widetilde{G}$ leaves the detector the photon travels to the detector wall and deposits energy in the EM calorimeter. A prompt photon would travel directly to the detector walls. Relative to the collision vertex time, the photon from the $\widetilde{\chi}_1^0$ would appear "delayed" in time. Note that the lifetime of the $\widetilde{\chi}_1^0$ may be long enough for it to leave the detector, giving rise to $\not\!\!E_T$.

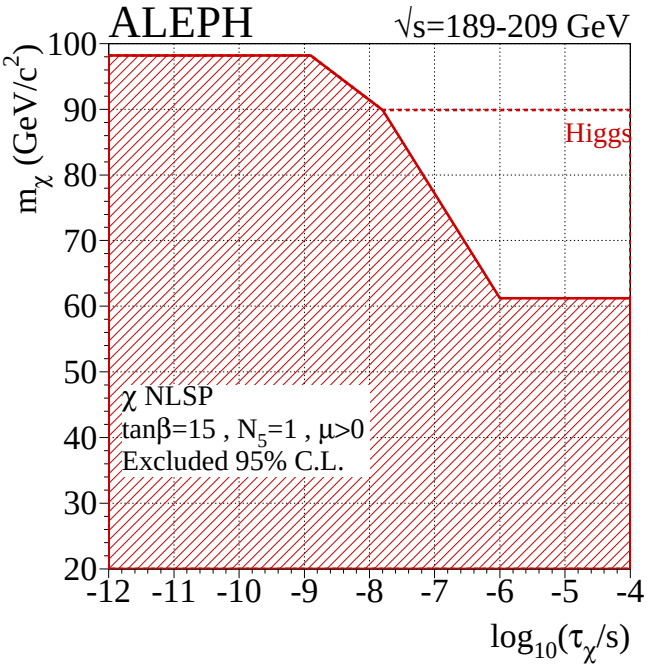

FIG. 2: The exclusion region from direct and indirect limits of GMSB searches at ALEPH/LEP [5] as a function of $\widetilde{\chi}_1^0$ mass and lifetime for the Snowmass Slope-choice of parameters [14]. The shaded region is from direct searches for GMSB $\widetilde{\chi}_1^0$ using photon pointing, the dashed line shows the indirect exclusion region from searches for the Higgs boson. $\widetilde{\chi}_1^0$ masses of less than 90 GeV/c^2 in GMSB models are excluded. There are additional limits from L3/LEP [7] but they are unpublished as of this writing.

II. THEORY

A major theory that predicts heavy, neutral, long-lived particles that decay to photons is GMSB [3]. It has 6 free parameters: the supersymmetry breaking scale, Λ, the messenger mass scale, $M_{\rm M}$, the ratio of the Higgs vacuum expectation values, $\tan(\beta)$, $\mathrm{sgn}(\mu)$, the number of messenger fields, $N_{\rm M}$, and the $\widetilde{G}$ mass factor, $c_{\rm Grav}$. In these models the NLSP is either the stau, $\widetilde{\tau}$, or the $\widetilde{\chi}_1^0$. For concreteness we use the Snowmass Slope constraint (SPS 8) [14] that is commonly used [5, 16] to reduce the number of free parameters from 6 to 2: the $\widetilde{\chi}_1^0$ mass and lifetime. We will focus on the $\widetilde{\chi}_1^0$-NLSP case here, for which the branching ratio is $\sim$100% to decay to a photon and a $\widetilde{G}$. At the Tevatron $\widetilde{\chi}_1^0$'s are mostly pair produced as end products of cascade decays from a chargino, $\widetilde{\chi}_1^{\pm}$, pair ($\sim$45% of all channels) or a $\widetilde{\chi}_1^{\pm}$ and a $\widetilde{\chi}_2^0$ ($\sim$25% of all channels) [15]. The major decay channels are shown in Fig. 3. For much of the parameter space the $\widetilde{\chi}_1^0$ can be long-lived, with a decay time on the order of nanoseconds which corresponds to decay lengths of meters. The $\widetilde{\chi}_1^0$ can decay inside the detector or, in a fraction of cases, leave the detector volume before it decays. This separates 3 event signatures: $\gamma\gamma + \not\!\!E_T$, $\gamma + \not\!\!E_T$, or $\not\!\!E_T$, each in association with jets from the τ's in the cascade decays. In this note we will focus on the $\gamma + \not\!\!E_T$ case as this (a) allows us to make use of the delayed arrival time of the photon and (b) is most sensitive to a large range of lifetimes on the order of nanoseconds [6].

Table I shows the GMSB model parameters, the resulting $\widetilde{\chi}_1^0$ mass and lifetime, and the next-to-leading-order (NLO) production cross section for example points. The production cross sections are calculated to leading-order using PYTHIA with the NLO corrections using the K-factors shown in Figure 4 as a function of $\widetilde{\chi}_1^0$ masses for $\widetilde{\chi}_1^{\pm}$ pair and $\widetilde{\chi}_1^{\pm}\widetilde{\chi}_2^0$ production [17]. The values range between 1.1-1.3 for the mass range considered. The production cross section is independent of the $\widetilde{\chi}_1^0$ lifetime, as this only scales with the $\widetilde{G}$ mass for a fixed $\widetilde{\chi}_1^0$ mass [3]. We use the total production cross section to estimate our sensitivity as it produces the best limits [18]. As shown in Fig. 2, for SPS 8 the ALEPH results show a lifetime dependent limit on the $\widetilde{\chi}_1^0$ mass of $\sim$60-98 GeV/c^2, the indirect lifetime independent limit from Higgs searches is 90 GeV/c^2 [5]. Next we outline our search strategy and the datasets.

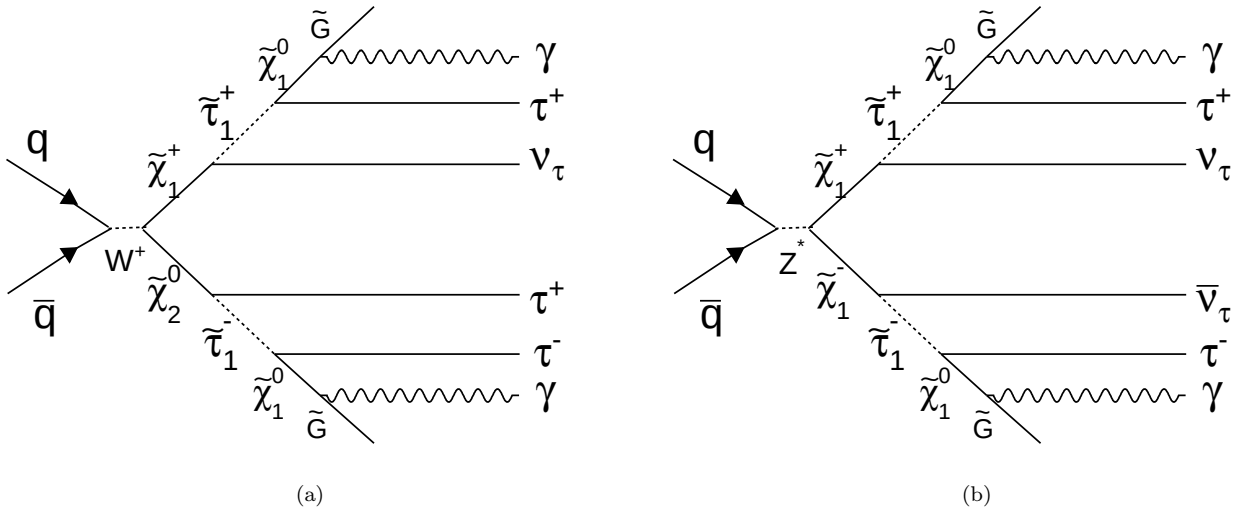

FIG. 3: Feynman diagrams of the dominant tree production processes at the Tevatron for the GMSB model line we consider: $\widetilde{\chi}_1^{\pm}\widetilde{\chi}_2^0$ (45%) (a) and $\widetilde{\chi}_1^{+}\widetilde{\chi}_1^{-}$ pair (b) production (25%). The τ's and second photons, if available, can be identified in the calorimeter as jets. Note that we only show one choice for the charge. The remaining processes are slepton (τ_1, e_R, μ_R) pair production.

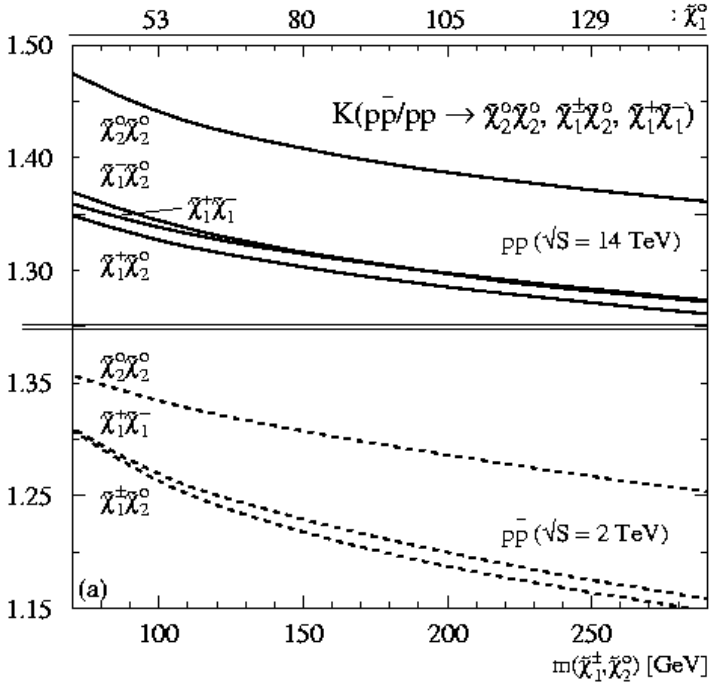

FIG. 4: The K-factors for use in modifying the LO production cross sections of $\widetilde{\chi}_1^+\widetilde{\chi}_1^-$ pair and $\widetilde{\chi}_1^\pm\widetilde{\chi}_1^0$ production from PYTHIA as a function of the average mass of the $\widetilde{\chi}_1^\pm$ and $\widetilde{\chi}_2^0$ which are almost identical in the scenario chosen in Ref. [14]. The figure is taken from Fig. 3a of Ref. [17]. For convenience we have plotted the $\widetilde{\chi}_1^0$ mass as a second x-axis, taken from Fig. 3b therein.

$m_{\widetilde{\chi}}$ (GeV/c^2)	$\tau_{\widetilde{\chi}}$ (ns)	$m_{\widetilde{G}}$ (eV/c^2)	Λ (GeV)	K-factor	NLO $\sigma_{\rm prod}$ (pb)
67	10	121	51500	1.23	1.26
80	10	199	60500	1.21	0.518
80	20	280	60500	1.21	0.518
100	5	248	74000	1.19	0.162

TABLE I: GMSB parameters example $\widetilde{\chi}_1^0$ masses and lifetimes relevant for this analysis and their translation to the SUSY parameters in accordance with the GMSB Snowmass Slope SPS 8 [14], and the NLO production cross sections. The production cross section is independent of the $\widetilde{\chi}_1^0$ lifetime, as this only scales with the $\widetilde{G}$ mass for a fixed $\widetilde{\chi}_1^0$ mass [3]. Note the different unit for the $\widetilde{G}$ mass.

III. OUTLINE OF THE SEARCH AND DATA SETS

A. Overview

This analysis is triggered on the photon and $\not\!\!E_T$ from the $\widetilde{\chi}_1^0$ decay by selecting events from the W_NOTRACK trigger which requires a central high-E_T EM-cluster and $\not\!\!E_T$. This set of events is then searched for a good photon, large $\not\!\!E_T$ and at least one high-p_T jet, presumably from the cascade decays from $\widetilde{\chi}_1^\pm$ and/or $\widetilde{\chi}_2^0$. Then we apply a baseline set of requirements to remove the dominant background sources as described in Section III C. The final signal region is defined by further kinematic cuts, described in Section VII, and finally a cut on the fully corrected photon arrival time [11] from the EMTiming system. The number of background events inside this timing window is estimated using a fit of the known shapes of the backgrounds in control regions outside the window of the same dataset as described in Section IV.

The main backgrounds to this analysis can be separated into two types of sources [9]: collision and non-collision background. The collision backgrounds mainly consist of events from QCD with fake $\not\!\!E_T$, with minor contributions of W + jets with the electron faking the photon. In these events the highest-$\Sigma p_{\rm T}$ vertex, reconstructed with an algorithm that is sensitive to the position and time of the tracks [10], does not coincide with the collision that produced the photon. The non-collision backgrounds consist of cosmic and beam halo sources [9].

In Sec. VII we optimize our predicted sensitivity using a simulation of the event distribution in the signal region from the GMSB model (see Sec. V) and calculate, for each GMSB parameter point the lowest, expected 95% C.L. cross section limit as a function of the following event variables: Photon E_T, $\not\!\!E_T$, jet E_T, $\Delta\phi(\not\!\!E_T, \text{jet})$ and $t^\gamma_{\rm corr}$. After the optimization we are left with an optimal, robust set of requirements that we apply when we unblind the signal region. We next describe the trigger and the dataset that is used for the baseline selection.

B. Triggers and Data Sets

We select central photons using the W_NOTRACK trigger for runnumbers in the range 190851-206989, starting when the EMTiming system became fully functional, using the Good Run list v11, which corresponds to a luminosity of (570±34) pb^{-1}. The trigger selection requirements are listed in Table II and include no isolation or CES-χ^2 requirements on the photon that might be inefficient for photons from long-lived particles [12]. The trigger is 100% efficient at EM cluster-E_T = 30 GeV and $\not\!\!E_T$ = 30 GeV [24], where we will set the baseline cuts for these variables. The events are reconstructed using Gen6 production and Stntuple dev_242.

Trigger Type	Level 1	Level 2	Level 3
	EM8_AND_MET15	CEM20_L1_MET15	W_NOTRACK_MET25
Photon	EM8:	CEM20:	Photon25:
	E_T (central) = 8 GeV	$\lvert\eta_{\rm max}\rvert$ = 1.1	CalorRegion = 2
	E_T (plug) = 8 GeV	E_T = 20 GeV	cenET = 25 GeV
	$E_{\rm Had}/E_{\rm Em}$ (central) = 0.125		cenHadEm = 0.125
	$E_{\rm Had}/E_{\rm Em}$ (plug) = 0.125	DCAS_HIGH_EM:	nEmObj = 1
	Photon Number = 1	central/forward/plug seed = 8 GeV	nTowersHadEm = 3
		central/forward/plug shoulder = 7.5 GeV	plugEt = 25 GeV
			plugHadEm = 0.125 GeV
$\not\!\!E_T$	MET15:		metCut25:
	$\not\!\!E_T$ = 15 GeV		MetCut = 25 GeV
	ΣE$_{\rm T}$ (central) = 1 GeV		
	ΣE$_{\rm T}$ (plug) = 1 GeV		

TABLE II: Triggers that contribute to the W_NOTRACK dataset and their requirements.

C. Baseline Event Selection

From the `W_NOTRACK` trigger events, we next create a baseline sample of $\gamma + \not\!\!E_T$ + jets events. We require one central photon with a corrected E_T>30 GeV which is where the trigger is fully efficient [24]. We select the highest-E_T photon in the event using standard Joint-Physics high-E_T photon cuts [25], but without the CES-χ^2 requirement as it has

been shown to be potentially inefficient for the signal [12], but with a requirement on the PMT asymmetry to reduce PMT spikes [9]. Additionally we require a raw $\not\!\!E_T$, corrected for the vertex, of $\not\!\!E_T \geq 30$ GeV, where the trigger is fully efficient, and at least one jet (cone R = 0.7), that does not match to the reconstructed photon, with a level 7-corrected $E_T > 30$ GeV and $|\eta| < 2.0$. This helps to reduce non-collision backgrounds. To create the fully corrected photon time we require the highest-$\Sigma p_{\rm T}$ vertex reconstructed with the space-time vertex algorithm [10] to have at least 4 good tracks that have a $\Sigma p_{\rm T}$ of at least 15 GeV/c. This also reduces non-collision backgrounds. We additionally use a standard cosmic ray cut [24] (muon co-stub cut) to further reject cosmic ray background. It rejects all events with no track attached to a muon stub within 30° of the photon. The full photon, jet and global event requirements as well as the vertex selection cuts that define our baseline sample are listed in Table III. The track selection criteria for the vertexing are listed in Table IV and are the standard cuts on COT tracks but with an additional $\frac{dE}{dx}$ cut to reject slow protons that spoil the vertex time measurement. Table V lists the cumulative number of events which pass each of the successive cuts to create our baseline sample. We show kinematic distributions and the final selection requirements after the optimization procedure in Section VII.

Requirement
Photon
$E_T > 30$ GeV
Fiducial: $\lvert X_{\rm CES}\rvert < 21$ cm && 9 cm $< \lvert Z_{\rm CES}\rvert < 230$ cm
$E_{\rm Had}/E_{\rm Em} < 0.125$
$E^{\rm Iso}_{\rm R=0.4} < 2.0 + 0.02 \cdot (E_T - 20)$
$N_{\rm trks} = 0$ or $N_{\rm trks} = 1$ and $p_T < 1.0 + 0.005 \cdot E_T$
$\Sigma p_{\rm T}$ of tracks in a 0.4 cone $< 2.0 + 0.005 \cdot E_T$
$E^{\rm cluster}_{\rm 2nd\ strip\ or\ wire} < 2.34 + 0.01 \cdot E_T$
PMT asymmetry: $\lvert E_{\rm PMT1} - E_{\rm PMT2}\rvert/(E_{\rm PMT1} + E_{\rm PMT2}) < 0.6$
Jet
$E_T^{\rm jet}$(cone 0.7) > 30 GeV, Jet Corrections level 7
$\lvert\eta^{\rm jet}_{\rm detector}\rvert < 2.0$
Vertex
Highest Σp_T space-time vertex with $N_{\rm trks} \geq 4$
$\Sigma p_{\rm T}$>15 GeV
$\lvert z\rvert < 60$ cm
Global Event Cuts
raw $\not\!\!E_T > 30$ GeV
μ co-stub cut, $\Delta\phi(\mu{-}{\rm stub}, \gamma)$>30°
Passes `W_NOTRACK` trigger

TABLE III: The photon, jet, vertex selection and global event cuts used to select the baseline sample of $\gamma + \not\!\!E_T + \geq 1$ jet events. Note that we use the standard photon ID cuts with the addition of a PMT asymmetry [9], but without a CES-χ^2 requirement [12]. The space-time vertexing is described in [10]. We use the track requirements shown in Table IV. The μ co-stub cut is explained in [24]. The number of events in the data that pass each cut are shown in Table V, the estimated signal acceptance in Table VI.

Requirement
$p_T > 0.3$ GeV
$p_T > 1.4$ GeV $\|\|$ $\frac{dE}{dx} < 20$, only if charge> 0
Err$(z_0) < 1$ cm
$\|\eta\| < 1.6$
NCotStSeg(5)$\geq$2
NCotAxSeg(5)$\geq$2
$\|t_0\| < 40$ ns
$0.05 <$ Err$(t_0) < 0.8$ ns
$\|z_0\| < 120$ cm

TABLE IV: Track requirements for the vertex reconstruction. These are the standard cuts but with an additional $\frac{dE}{dx}$ cut to reject slow protons that spoil the vertex time measurement.

Selection	No. of Observed Events
$E_T > 30$, $\not\!\!E_T > 30$, photon ID cuts	119944
Good vertex, $\Sigma P_{\rm T} > 15$ GeV/c	19574
$\geq$1 jet with $E_T > 30$ GeV and $\|\eta\| < 2.0$	13097
Cosmics rejection (μ co-stub)	12855

TABLE V: Event reduction for the baseline $\gamma + \not\!\!E_T +\geq 1$ jet dataset. The total Good Run-luminosity before any of above cuts, after the trigger (see Table II), is (570$\pm$34)pb^{-1}. For the individual requirements see Table III.

IV. BACKGROUND METHODS

A. Overview

The final signal region for this analysis is defined by the subsample of events that passes a set of final kinematic and timing window cuts. The method for determining the background in the signal region is based on data alone and uses timing control region subsamples, and timing shape templates for each of the background sources [9]. Each of these subsamples is drawn from the baseline sample (defined in the previous section) and selected using timing and additional kinematic cuts. Then, using fits of the templates to the control regions we normalize the amount of background from each source and then use the templates to extrapolate to the number of background events in the final timing window. Since the method is based on the timing distributions alone we can create background estimates for a large number of potential signal regions, each corresponding to different sets of kinematic and final timing cuts. In other words, given a subsample defined by kinematic cuts alone we can estimate the number of background events in a potential signal timing window. Thus, we can predict the backgrounds for a large variety of final sets of cuts and use these estimates as part of the optimization procedure described in Sec. VII. In this section we describe the backgrounds, the timing control regions and the methods used to estimate the backgrounds for all these various potential signal regions. The final kinematic cuts used in the optimization procedure are described in Sec. VII.

There are two background sources [9]: photon candidates from collision sources, and photon candidates from non-collision sources such as cosmic rays and beam halo. Figure 5 shows the time shapes for each background. The region around 0 ns is dominated by collision data, while large positive times are dominated by cosmic rays (flat in time), and negative times are dominated by beam halo. To create a separate control region for each of the three backgrounds (cosmics, beam halo or collision data) and minimize the correlation between them in the final background estimate methods we use the expected timing distributions from Fig. 5. The cosmics timing distribution is essentially flat in time so our control region is defined to be [25,90] ns and is chosen such that (a) it is well above the beam halo secondary peak at $\sim$ 18 ns [9] and (b) does not not include the region close to the end of the ADMEM energy integration gate where the event rate falls sharply. (Between 90 ns and 110 ns not all the energy deposited in the calorimeter is integrated and leads to a gross energy mismeasurement, causing the rate to drop.) The beam halo control region [-20,-6] ns is chosen such that (a) it contains most of the beam halo events but (b) stays well away from the region dominated by the prompt photon production. The collision data region is defined to be [-10,1.2] and is chosen such that (a) we include as much of the collision data as possible to get the ratio of right to wrong vertices as accurately as possible, and (b) is below the final signal region of [2,10] ns. The lower limit of 2 ns is chosen as part of the optimization (see Section VII). While the precise upper time limit of the signal region at 10 ns is not quantitatively motivated, most of a long-lived signal on the order of ns lifetimes is included in this interval as shown in Fig. 9 of Ref. [11]. While we describe each background below and outline the methods for estimating their rate, Ref. [9] describes each in more detail.

The background prediction for each subsample of events after kinematics cuts is done as a two-step process. The first step is to estimate the contributions from the right and wrong vertex collision background and take into account non-collision contamination. The second step is to use the the collision shapes to estimate the non-collision backgrounds using a simultaneous fit. For step 1, the right and wrong vertex background is estimated using the timing control window [-10,1.2] ns (expected to be dominated by collision data), but excluding wedges other than 0 and 23 which contains the bulk of the beam halo contribution [9]. The non-collision contamination is estimated by fitting the beam halo and cosmics templates simultaneously in the control regions [-20,-6] ns (beam halo dominated) and [25,90] ns (cosmics dominated), and extrapolating to the collision control region [-10,1.2] ns, where they are subtracted off. The remaining data is then fit by allowing the fraction of right to wrong vertices to float, and then scaling by a factor of 24/22 to account for the data in wedges 0 and 23. For step 2, a fit for the normalization is performed for all wedges in the beam halo and cosmic ray timing control regions and subtracting off expected contamination from collision sources to determine the rate of the non-collision backgrounds.

The following subsections outline how each of the background shapes are obtained and how the background, and error, is estimated in the final signal timing window.

B. Non-Collision Backgrounds

As described in Ref. [9], to generate our non-collision time shape templates we use data from the W_NOTRACK trigger. Events with photon candidates passing all of the photon ID cuts in Table III are selected. We then require no track activity by applying a cut of $\Sigma p_{\mathrm{T}}^{\mathrm{trk}} < 1$ GeV to select a sample of non-collision events.

A subsample of cosmics events is separated from beam halo events by applying the following additional cuts:

$$\text{wedge} \neq 0 \textit{ and } \text{wedge} \neq 23,$$
$$\text{nHadTowers} = 0 \textit{ and } \text{nEmTowers} < 5,$$

where nHadTowers is the total number of plug towers with hadronic energy > 0.1 GeV in the same wedge as the photon candidate and nEmTowers the total number of central towers with electromagnetic energy > 0.1 GeV in the same wedge as the photon candidate.

The subsample of beam halo events is selected by requiring:

$$\text{nHadTowers} > 1 \textit{ and } \text{nEmTowers} > 4 \text{ for all wedges},$$
$$\text{no muon stubs}$$

where the muon stubs removal further reduces any possible contamination from cosmics. The timing distribution for both samples of events is shown in Fig. 5b.

Once the histogrammed time shape templates for both backgrounds are established, the fit for the normalization is performed to match the total number of the events in the kinematics-only sample, in the two control regions of [-20,-6] ns (dominated by beam halo), and [25,90] ns (dominated by cosmics). The number of events of both backgrounds are allowed to float independently such that the result of the fit gives the total number of events in the control regions from each of the non-collision backgrounds. This determines the predicted number of events in the signal and collision regions. The errors assigned to the prediction are taken from the fit and take into account the correlation matrix.

C. Collision Backgrounds

The shape of the collision background for right and wrong vertices is estimated from $W \rightarrow e\nu$ data where the electron track is dropped from the vertexing to closely mimic events with photons [9] and shown in Fig. 5a. Once the total number and shape of the non-collision backgrounds is established for a kinematics-only sample, the fit to the collision data is performed. Both shapes for the wrong and right vertex events are fixed using the Gaussian functions according to [9], in particular the mean and RMS, and only the relative normalization between the two is allowed to float. At the end of the fit the statistical error on the prediction for a signal region is determined by the fit and takes into account the correlation matrix. The systematic uncertainty on the number of events in the signal time window is estimated by varying the mean and RMS of the collision background timing shapes. As discussed in Ref. [11] the mean of the timing distribution can vary between data samples. From $W \rightarrow e\nu$ events we conservatively overestimate the potential shift to be 200 ps on the primary Gaussian. Similarly, the RMS of the primary distribution can vary by the amount of the fit uncertainty to the corrected time distribution of the $W \rightarrow e\nu$ sample (0.02 ns) [11]. The dominant uncertainty on the secondary Gaussian of the prompt timing distribution is due to a geometric effect as described in Ref. [9], and conservatively overestimated to be and 330 ps on the mean and 280 ps on the RMS.

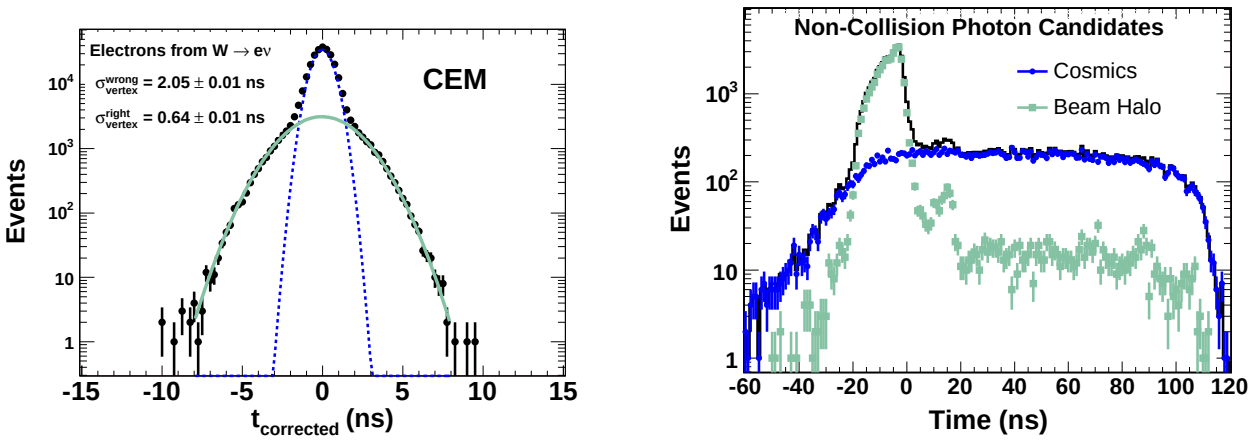

(a) (b)

FIG. 5: The background shapes as a function of time, separated into collision (a) and non-collision (b) backgrounds. Figure (a) shows the $t^{\gamma}_{\rm corr}$ distribution of collision data for right and wrong vertex selections, as estimated using a sample of electrons from $W \rightarrow e\nu$ where the electron track has been ignored. Figure (b) shows the cosmics and beam halo background shapes obtained from the non-collision sample described in Section IV B, separated with the additional wedge, nHadTowers and nEmTowers cuts.

V. ACCEPTANCE AND EFFICIENCIES FOR GMSB MODELS

In this section we describe the MC simulation of the GMSB model, and how we estimate our signal acceptance. We point out how we take effects into account that are not simulated and show the GMSB signal efficiency to pass various sets of cuts. We use the PYTHIA event generator and *cdfSim* of *cdfsoft* release 6.1.2 [11, 27] with the default settings, modified for the simulation of the EMTiming system (see App. B in Ref. [12]). We simulate the full GMSB model with the setting MSEL=39 with the masses calculated with ISASUGRA [28]. We use the detector calibrations of runnumber 191636 for all MC samples. Each sample contains 120000 events which yields a statistical uncertainty of $\sim 1\%$ if the probability for signal events to pass our cuts is $\sim$5%.

The total event efficiency is used when calculating the cross section limits, and is given by:

$$A \cdot \epsilon = (A \cdot \epsilon)_{\text{Signal MC}} \times C_{\text{MC}} \tag{1}$$

where A is the acceptance, ϵ the efficiency and C_{MC} a correction factor to the MC simulation for small effects that are not simulated in the MC. While the photon ID efficiencies and the EMTiming system resolution have been shown to be correctly simulated for prompt electrons and for photons from long-lived particles in [11, 12], the MC does not simulate (1) multiple collision effects and (2) cosmic ray backgrounds.

Multiple collisions in the event can produce an extra vertex that would be incorrectly picked as the events vertex. To take this effect into account we simulate fake vertices by varying the z_0 and the t_0 of the vertex randomly with Gaussians of $\sigma_z = 30$ cm and $\sigma_t = 1.3$ ns, respectively. We assume the wrong vertex fraction of events to be (3±1)%, a number that has been obtained by the background estimate (see Section IV). This is a conservative estimate as the average vertex Σp_{T} for GMSB is higher than for QCD events that dominate the SM background. In Section VI we show that varying this number has a negligible impact on the acceptance.

The fraction of GMSB events lost due to a cosmic ray overlapping our event and causing the μ co-stub cut to fail our requirements is not simulated in the MC. This is estimated by multiplying $A \cdot \epsilon$ with the efficiency of the muon co-stub cosmics rejection cut that we measure directly from our data sample. We estimate this by applying the baseline cuts on our data sample and require the photons to be within $|t^{\gamma}_{\text{corr}}| < 10$ ns to select collision events with high purity. There are 12583 events in this sample. As we show later this sample has a negligible contribution from cosmics (see Table XI). We find that 12360 events remain after the cosmics rejection cut, giving an efficiency of $C_{\text{MC}} = 12360/12583 = (98.2 \pm 1)\%$, with the error conservatively overestimated.

The breakdown of events after passing each of the event and object baseline selection cuts in Table III for an example GMSB point at $m_{\tilde{\chi}} = 100$ GeV and $\tau_{\tilde{\chi}} = 5$ ns is shown in Table VI. The results for other cuts used in the optimization and final event selection are given in Sections VII and VIII.

Requirement	Events passed	$(A \cdot \epsilon)_{\text{Signal MC}}$ (%) ($m_{\tilde{\chi}} = 100$ GeV and $\tau_{\tilde{\chi}} = 5$ ns)
Sample events	120000	100.00
Central photon with $E_T > 30$, $\not\!\!E_T > 30$	64303	53.6
Photon fiducial & ID cuts	46730	38.9
Good vertex	37077	30.9
≥1 jet with $E_T > 30$ GeV and $\|\eta\| < 2.0$	28693	23.9
μ co-stub cut ($\times C_{\text{MC}}$)	N/A	23.5

TABLE VI: Summary of the event reduction for a GMSB example point in the $\gamma + \not\!\!E_T +$ ≥ 1 jet final state as we place the baseline cuts of Table III. Note that the μ co-stub cut is implemented as an MC correction factor, C_{MC}.

VI. ESTIMATION OF THE SYSTEMATIC UNCERTAINTIES

In order to estimate the sensitivity of the search we calculate the expected 95% C.L. cross section limits, which involves the uncertainties in the luminosity, background, acceptance and GMSB production cross section. The systematic uncertainty on the luminosity is considered to be 6% at CDF with major contributions to the CLC acceptance from the precision of the detector simulation and the event generator [29]. The uncertainty on the background in the signal region is determined from our understanding of the collision and non-collision sources from the control regions. It is estimated from $W \to e\nu$ and non-collision events, as described in Section IV. The acceptance and cross section uncertainties are estimated in the subsections below. To summarize, the systematic uncertainty on the acceptance-MC sample is estimated to be 8.8% with major contributions from the uncertainty on the timing distribution and the ID efficiency. We calculate the uncertainty on the NLO production cross section from PDF and the renormalization scale to be 6.4% and include this in the final cross section limit plots. The uncertainties on acceptance and cross section are summarized in Table VII for an example GMSB point of $m_{\tilde{\chi}} = 94$ GeV and $\tau_{\tilde{\chi}} = 10$ ns. For the optimization and limit setting we use a combined uncertainty of 10% on the acceptance and production cross section [30]. All uncertainties are consistent with the GMSB diphoton analysis [16], except the ISR/FSR uncertainty, as that analysis requires two prompt photons while this analysis requires one delayed photon and a jet which is less sensitive to ISR/FSR.

Factor	Relative Systematic Uncertainty (%)
Acceptance:	
Time distribution and vertex selection	6.7
Photon ID efficiency	5.0
Jet energy	3.0
ISR/FSR	2.5
PDF	0.7
Total	8.8
Cross section:	
PDF	5.9
Renormalization scale	2.4
Total	6.4

TABLE VII: Summary of the systematic uncertainties on the acceptance and production cross section for an example GMSB point at $m_{\tilde{\chi}} = 94$ GeV and $\tau_{\tilde{\chi}} = 10$ ns. For the optimization we combine in quadrature and take a 10% uncertainty on the acceptance. The estimation procedures are described in detail in the subsections of Section VI.

A. Mean and RMS of the Time Distribution and Vertex Selection

There is a potential systematic error on the acceptance if the timing distributions is also not simulated correctly. We consider simultaneously three types of uncertainties to the time distribution that affect the acceptance: (1) a shift in the mean in the time distribution, (2) a change in the RMS of the time distribution and (3) a change in the fraction of events from a wrongly chosen vertex.

As discussed in Ref. [11] the mean of the the timing distribution can vary between data samples. From $W \to e\nu$ events we measure the shift for a set of cuts to be 110 ps and conservatively overestimate the potential shift for this sample for varying cuts to be 200 ps. The fractional variation in the acceptance due to this shift is estimated to be 6.7%. Similarly, the RMS of the distribution can vary by the amount of the fit uncertainty to the primary corrected time distribution of the $W \to e\nu$ sample (0.02 ns) [11]. The fractional change in acceptance due to this effect is estimated to be 0.03%. The fraction of events for which the wrong vertex is picked has been estimated to be (3±1)% as described in Section V. We vary the fraction of events with the wrong vertex by the uncertainty of the fit to the negative time side of the data distribution (1%) and obtain an uncertainty of 0.1%. Varying the wrong vertex fraction between 0% and 10% we get an uncertainty of $< 1.5\%$. The systematic timing uncertainty is then the orthogonal sum of the uncertainties of each effect, 6.7%. This makes the major contribution to the systematic uncertainty.

B. Photon ID Efficiency

We take a systematic uncertainty of 5.0% for the photon ID efficiency as described in Ref. [12].

C. Jet Energy

As we allow jets with a corrected E_T of > 30 GeV in our set of events we have studied the change in acceptance if the jet energy is mismeasured. The following effects are taken into account: relative jet energy, underlying event, multiple interaction, absolute energy scale, out-of-cone and splash-out. The standard procedure at CDF [19] varies each correction factor independently by $\pm 1\sigma$. The resulting variation in the acceptance is $\pm 3.0\%$.

D. ISR/FSR

Initial and final state radiation (ISR/FSR) affects the E_T distributions of the products of the collision. To estimate the uncertainty we vary the Sudakov parameters as described in [20] and get a 2.5% variation in the acceptance.

E. Structure Functions (PDFs)

We use CTEQ-5L in this analysis. The structure functions uncertainty affects both the acceptance and the production cross section of the signal. Each is estimated by reweighting the parton momenta using the PDF uncertainties from CTEQ-6M as described in [21]. For the example GMSB point we get a relative uncertainty of $+0.7\%$ -0.5% [22] on the acceptance and $+5.9\%$ -5.3% on the cross section. We take the larger value of each to estimate the uncertainty conservatively.

F. Renormalization Scale

In PYTHIA [27] events are generated using a fixed renormalized (q^2) scale of $\hat{s}$. However, the NLO cross section, which is calculated with PROSPINO2 [23], varies as a function of the renormalization scale. The variation of the NLO production cross section from changing the scale from $0.25 \cdot q^2$ to $4 \cdot q^2$ is calculated with PROSPINO2 to be 2.4% for the example GMSB point and is consistent with the results in [16].

VII. OPTIMIZATION AND EXPECTED LIMITS

Now that the background is estimated and the signal acceptance is available for a given set of cuts, along with both uncertainties, an optimization procedure can be readily employed to find the optimal cuts before unblinding the signal region. We optimize for the following cuts: photon E_T, $\not\!\!E_T$, jet E_T, $\Delta\phi(\not\!\!E_T, \text{jet})$ and the lower limit on t^{γ}_{corr}, while fixing the upper limit at 10 ns. We optimize for all requirements simultaneously at each GMSB parameter point. Once we have the optimal values at each point we then decide for a set of cuts that we deem robust enough to be applied throughout the parameter space for simplicity.

By estimating our sensitivity using the 95% C.L. expected cross section limits on GMSB models, we can use the same method to also find the optimal set of cuts before unblinding the signal region. We use the standard cross section limit calculator [30] to calculate the limits, taking into account the predicted number of background events, the acceptance, the luminosity and their systematic uncertainties (see Section VI). We take

$$\sigma^{95}_{\text{exp}} = \sum_{N_{obs}=0}^{\infty} \sigma^{95}_{\text{obs}}(\text{cut})\ \text{Prob}(N_{obs}, N_{exp} = \mu) \tag{2}$$

$$\text{RMS}^2 = \sum_{N_{obs}=0}^{\infty} (\sigma^{95}_{\text{obs}}(\text{cut}) - \sigma^{95}_{\text{exp}})^2\ \text{Prob}(N_{obs}, N_{exp} = \mu) \tag{3}$$

where N_{obs} is the number of observed events in the pseudoexperiment, μ is the mean of the number of expected events as a function of the cuts and σ^{95}_{obs} denotes the cross section limit if N_{obs} were observed, and is also a function of the cuts.

The expected cross section limit is then a function of the cuts that we choose to optimize for (photon E_T, $\not\!\!E_T$, jet E_T, $\Delta\phi(\not\!\!E_T, \text{jet})$ and t^{γ}_{corr}), and has at each GMSB point a minimum for a set of optimal cuts. As an illustration of the optimization, Figure 6 shows the expected cross section limit as a function of the t^{γ}_{corr} cut, where we after keep all other cuts fixed at the (already) optimized values. Note that, in reality, we optimize for all cuts simultaneously. Table VIII lists the optimization results for all points in parameter space that are used for the optimization, along with the NLO production cross section at each point. There is only small variation in the jet E_T cut and the lower limit on t^{γ}_{corr} while all other requirements are constant over the points. We decided to use a single set of cuts before we open the box based with the expectation that they will yield the largest expected exclusion region. We chose: Photon E_T>30 GeV, jet E_T>35 GeV, $\Delta\phi(\not\!\!E_T, \text{jet})$>1.0, $\not\!\!E_T$>40 GeV and t^{γ}_{corr}>2.0 ns. We predict 1.3±0.7 background events with 0.46±0.26 from beam halo, 0.07±0.05 from cosmics, and 0.71±0.60 from SM, where we pick the wrong vertex in (0.56±0.24)% of the cases [26]. Table IX shows the expected and observed cross section limits, acceptance and production cross section of each GMSB point simulated, along with the predicted background, with the fixed set of optimized cuts. In each case a comparison with Table IX shows only small loss of sensitivity by using one fixed set of cuts.

Figures 7 and 8 show the distributions of each optimization variable normalized to the number of expected events, after applying all optimized cuts. We compare the background distribution before unblinding the signal region and the expected signal in the signal region for an example GMSB point at $m_{\tilde{\chi}} = 100$ GeV and $\tau_{\tilde{\chi}} = 5$ ns. Taking into account the errors we expect an acceptance of (6.3±0.6)% and 5.7±0.7 events for this point. Next we unblind the signal region and set limits for GMSB models and describe model-independent features.

	GMSB model $m_{\tilde{\chi}}$,$\tau_{\tilde{\chi}}$ (GeV/c^2, ns)										
	67,25	75,3	75,10	75,20	80,20	94,5	94,10	94,20	100,5	100,15	113,5
Photon E_T	30										
$\not\!\!E_T$	40										
Jet E_T	25	35	25	25	25	35	35	35	35	35	40
$\Delta\phi(\not\!\!E_T, \text{jet})$	1.0										
Lower limit on t^{γ}_{corr}	2.0	1.75	2.0	2.0	2.0	2.0	2.0	2.0	2.0	2.0	2.0
Acceptance (%)	0.9±0.1	3.0±0.3	2.6±0.3	1.6±0.2	2.1±0.2	5.3±0.5	3.9±0.4	2.4±0.2	6.3±0.6	3.6±0.4	8.1±0.8
Backgrounds:											
Prompt SM	1.0±0.7	1.6±1.7	1.0±0.7	1.0±0.7	1.0±0.7	0.7±0.6	0.7±0.6	0.7±0.6	0.7±0.6	0.7±0.6	0.7±0.6
Beam Halo	0.4±0.1	0.1±0.1	0.4±0.1	0.4±0.1	0.4±0.1	0.1±0.1	0.1±0.1	0.1±0.1	0.1±0.1	0.1±0.1	0.04±0.03
Cosmics	1.5±0.5	0.5±0.3	1.5±0.5	1.5±0.5	1.5±0.5	0.5±0.3	0.5±0.3	0.5±0.3	0.5±0.3	0.5±0.3	0.2±0.2
σ^{exp}_{95} (pb)	1.12	0.320	0.388	0.650	0.494	0.152	0.204	0.329	0.128	0.222	0.0935
NLO $\sigma_{\text{Signal MC}}$ (pb)	1.26	0.736	0.736	0.736	0.518	0.235	0.235	0.235	0.162	0.162	0.0824

TABLE VIII: The optimized cut values for each GMSB parameter point used in the optimization. All optimal values are quite stable as a function of $m_{\tilde{\chi}}$ and $\tau_{\tilde{\chi}}$. The $\not\!\!E_T$ goes slightly up and the $\Delta\phi(\not\!\!E_T, \text{jet})$ slightly down for higher $m_{\tilde{\chi}}$. As we expect our exclusion limit to be close to 100 GeV/c^2, we chose these values for the final signal region.

$m_{\tilde{\chi}}$	$\tau_{\tilde{\chi}}$	Acceptance (%)		Background	$\sigma_{95}^{\rm exp}$ (pb)		$\sigma_{95}^{\rm obs}$ (pb)		$\sigma_{\rm prod}$ (pb)
(GeV/c^2)	(ns)	MC	Fit		MC	Fit	MC	Fit	
67	1	0.77±008	0.97		1.05	0.826	1.25	0.984	
67	7	1.5±0.2	1.6		0.521	0.512	0.621	0.611	
67	10	1.4±0.1	1.3		0.581	0.610	0.693	0.727	
67	18	0.9±0.1	0.88		0.940	0.914	1.12	1.09	1.26
67	25	0.7±0.1	0.67		1.23	1.20	1.47	1.43	
67	35	0.5±0.1	0.50		1.62	1.61	1.93	1.91	
67	50	0.3±0.0	0.36		2.81	2.23	3.35	2.65	
75	0	0.3±0.0	0.27		2.64	2.95	3.15	3.52	
75	1	1.2±0.1	1.4		0.693	0.585	0.825	0.698	
75	3	2.5±0.2	2.5		0.321	0.318	0.383	0.379	
75	7	2.5±0.2	2.3		0.328	0.342	0.390	0.407	
75	10	2.1±0.2	2.0	1.3±0.7 (2 observed)	0.390	0.404	0.464	0.481	0.736
75	14	1.6±0.2	1.6	SM: 0.71±0.60	0.500	0.499	0.596	0.595	
75	20	1.2±0.1	1.2	BH: 0.07±0.05	0.674	0.651	0.804	0.776	
75	40	0.6±0.1	0.68	CS: 0.46±0.26	1.30	1.18	1.55	1.41	
75	100	0.3±0.0	0.29		2.90	2.80	3.46	3.34	
80	1	1.4±0.1	1.7		0.569	0.479	0.679	0.571	
80	3	3.3±0.3	3.2		0.245	0.254	0.292	0.303	
80	7	3.1±0.3	3.0		0.262	0.269	0.312	0.320	0.518
80	10	2.6±0.3	2.5		0.311	0.316	0.371	0.376	
80	15	1.9±0.2	2.0		0.424	0.408	0.506	0.486	
80	20	1.6±0.2	1.6		0.497	0.505	0.592	0.602	
84	5	3.9±0.4	3.7		0.207	0.216	0.247	0.257	0.402
94	0	0.5±0.1	0.47		1.73	1.73	2.06	2.06	
94	1	2.2±0.2	2.4		0.364	0.334	0.434	0.399	
94	3	5.1±0.5	4.8		0.157	0.169	0.187	0.201	
94	5	5.3±0.5	50		0.152	0.160	0.181	0.191	0.235
94	10	3.9±0.4	4.0		0.204	0.199	0.243	0.237	
94	20	2.4±0.2	2.6		0.329	0.313	0.392	0.373	
94	30	1.7±0.2	1.8		0.465	0.435	0.554	0.519	
94	40	1.3±0.1	1.4		0.625	0.560	0.745	0.667	
100	5	6.3±0.6	5.9		0.128	0.136	0.153	0.162	0.162
100	15	3.6±0.4	3.8		0.222	0.212	0.264	0.253	
113	0	0.56±0.1	0.61		1.42	1.31	1.70	1.56	
113	5	8.5±0.9	7.7		0.0944	0.105	0.112	0.125	0.0824
113	10	6.6±0.7	6.4		0.122	0.125	0.145	0.149	

TABLE IX: The acceptance and expected cross section limits for various simulated GMSB points for the final selection requirements. "BH" and "CS" denote beam halo and cosmics background, respectively. The acceptances in the column marked "Fit" are obtained using the interpolation functions described in more detail in Section VIII B. For completeness, we have included both the expected and observed number of events and cross section limits from Section VII.

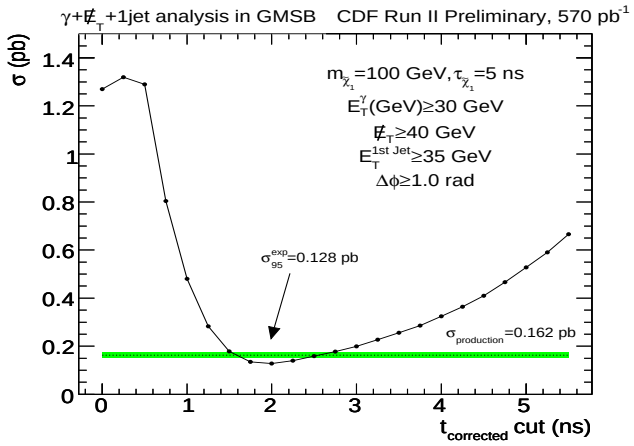

(a)

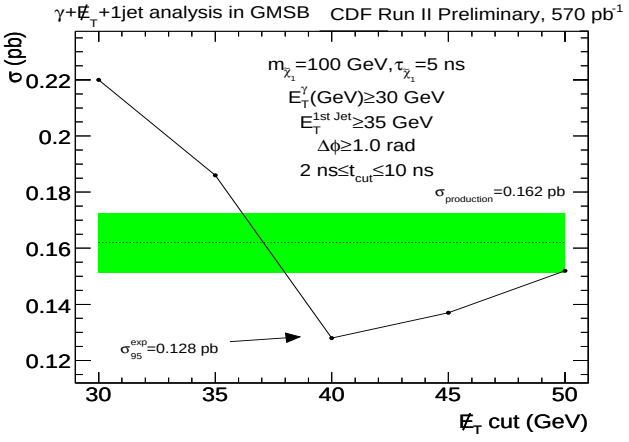

(b)

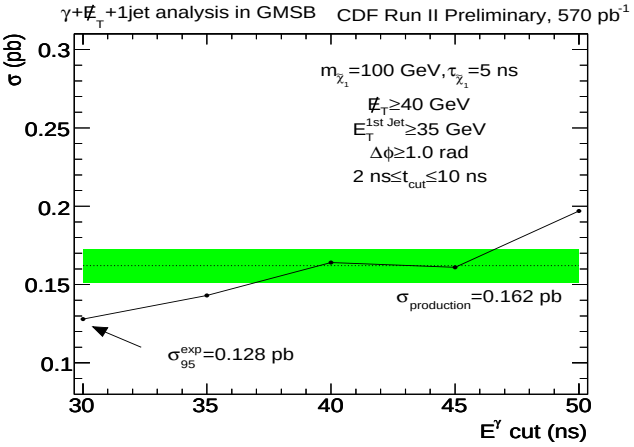

(c)

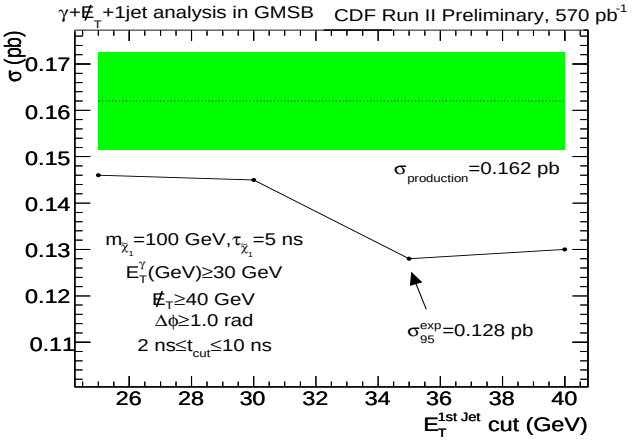

(d)

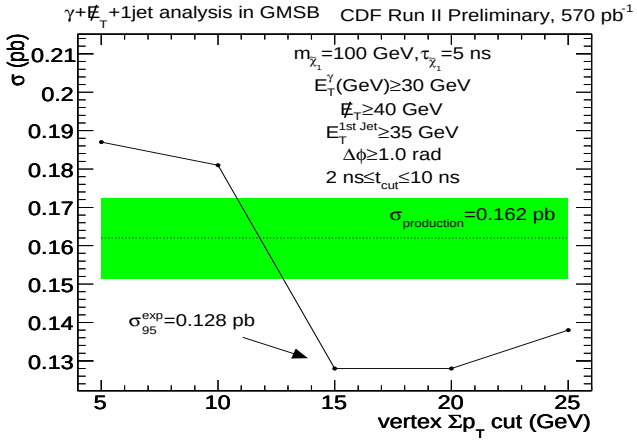

(e)

FIG. 6: The expected 95% C.L. cross section limit as a function of the $t^{\gamma}_{\rm corr}$, the $\not\!\!E_T$, the photon E_T, the vertex $\Sigma p_{\rm T}$ and the jet E_T requirement for a GMSB example point ($m_{\tilde{\chi}} = 100$ GeV and $\tau_{\tilde{\chi}} = 5$ ns). The optimal point is where the expected cross section is minimized. Indicated in green is the 6.5% uncertainty-band for the production cross section (see Table VII). The arrows show the choices of the final cuts, and the expected cross section limit values.

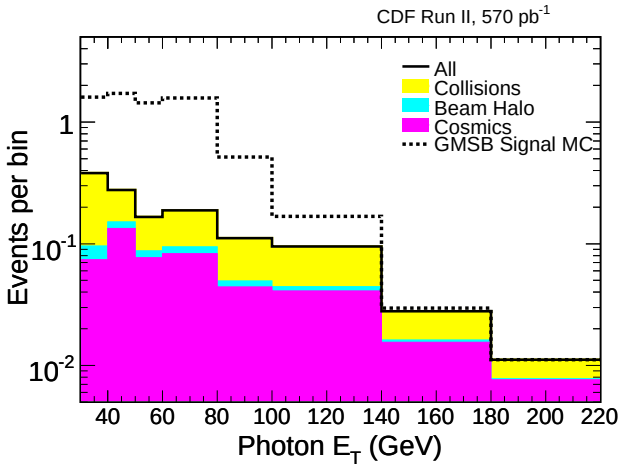

(a)

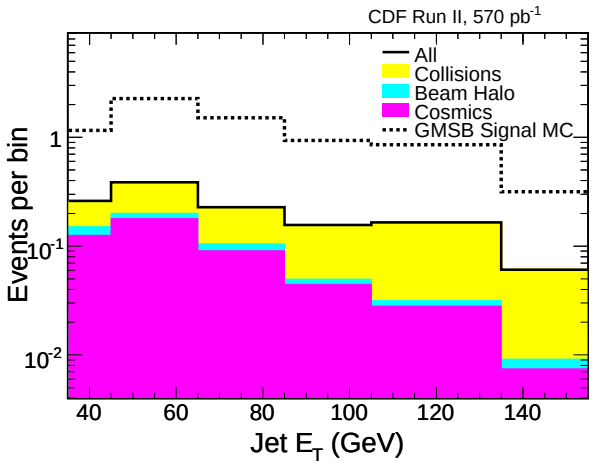

(b)

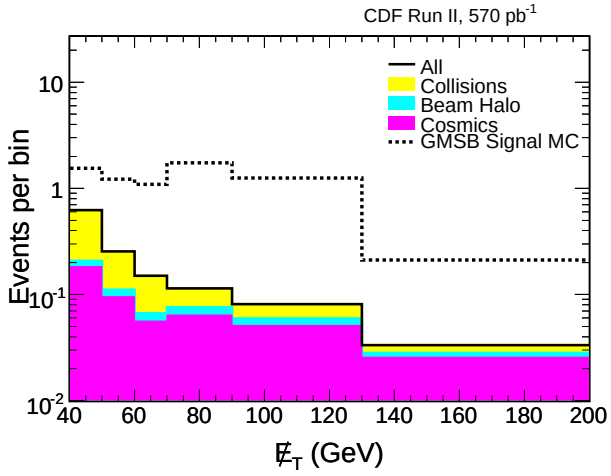

(c)

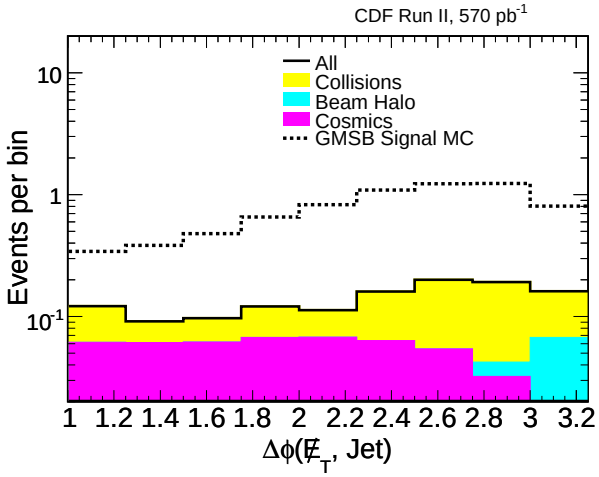

(d)

FIG. 7: The predicted kinematic distributions in the signal region after the baseline and optimized requirements. We compare the background prediction for the signal region and the GMSB signal, for an example point at $m_{\tilde{\chi}} = 100$ GeV and $\tau_{\tilde{\chi}} = 5$ ns. We predict 1.3±0.7 background events after all cuts. The MC is normalized to the number of expected signal events, 5.7±0.7.

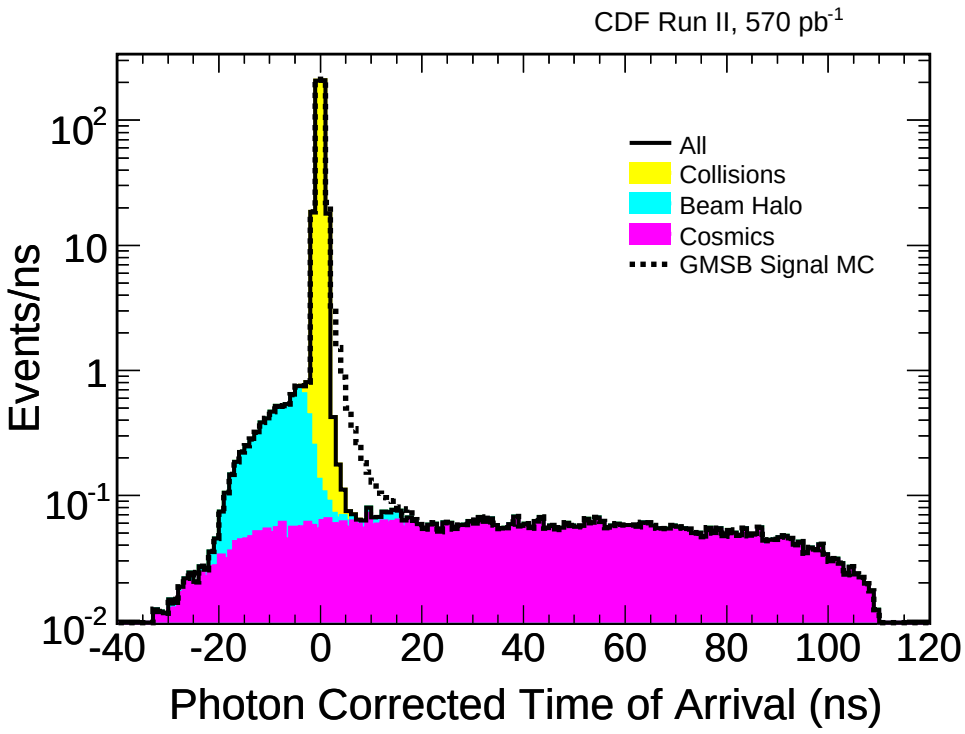

(a)

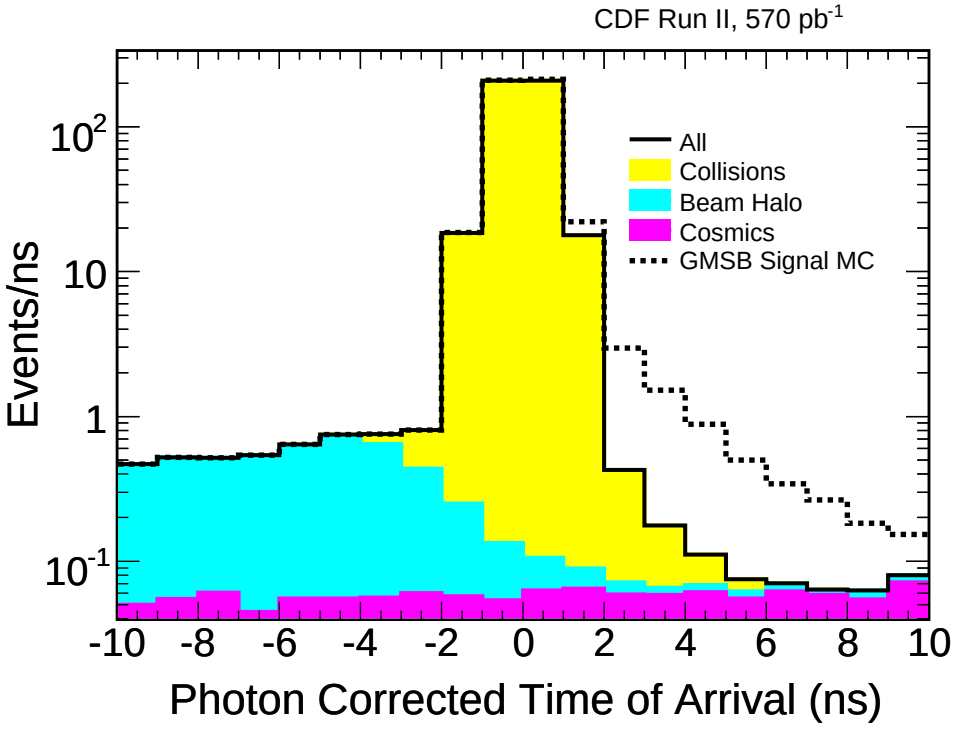

(b)

FIG. 8: The predicted time distribution in the full time window and around the signal region, after passing the baseline and optimized kinematic cuts. We compare the background prediction for the signal region and the GMSB signal, for an example point at $m_{\tilde{\chi}} = 100$ GeV and $\tau_{\tilde{\chi}} = 5$ ns. We predict 1.3±0.7 background events after all cuts in the signal region $2\text{ns} \leq t^{\gamma}_{\text{corr}} \leq 10$ ns. The MC is normalized to the number of expected signal events, 5.7±0.7.

VIII. DATA, CROSS SECTION LIMITS, RESULTS AND CHECKS

In this section we unblind the signal region, set model-independent cross section limits and show exclusion regions for GMSB models. We describe a parametrization of model-independent features of the acceptance.

A. The Data

After all kinematic cuts there are 508 events in the data. Figure 9a shows the data along with the signal expectations and the background shapes at all times, including the control regions. Table X lists the number of events observed in the three control regions; the fits to the shape templates predict 6.2±3.5 events from cosmics, 6.8±4.9 events from beam halo and the rest from SM. To check the background estimation methods, Table XI lists the expected number of background and signal events for a GMSB example point as each of the optimized requirements is applied one at a time. Note that the predictions are for the loose timing window 1.2ns $\leq t^{\gamma}_{\rm corr} \leq$ 10 ns to allow the background method to make predictions at each stage for comparison. In other words, each of the numbers in this table is based on control region measurements and is not biased. Also note that the bulk of the beam halo and cosmics background is rejected by the timing requirement. At each requirement a GMSB signal would have increased the number of events observed in the signal region but there is a good agreement between background prediction and the number of events observed.

There are 2 events in the final signal region, $2 < t^{\gamma}_{\rm corr} < 10$ ns, consistent with the background expectation of 1.3±0.7 events. Figure 9b shows a blow up of the timing window and again shows consistency with expectations. Figure 10 shows the kinematic distributions of our events along with the predictions and also shows consistency. There is no distribution that hints at an excess and the data appears to be well modeled by the background predictions. For completeness we present the acceptance as a function of the cuts in a slightly different order for $m_{\tilde{\chi}} = 100$ GeV and $\tau_{\tilde{\chi}} = 5$ ns in Table XII, in the way it is shown in the PRL paper.

Control Region	Dominant Background	Observed Events
$-20 \leq t^{\gamma}_{\rm corr} \leq -6$ ns	Beam halo	4
$-10 \leq t^{\gamma}_{\rm corr} \leq 1.2$ ns	SM	498
$25 \leq t^{\gamma}_{\rm corr} \leq 90$ ns	Cosmics	4

TABLE X: The observed number of events in each control region after all optimized cuts, except the timing cut, as shown in Fig. 9. Each is used to estimate the number of events in the signal region. We observe 508 events in the total time window and 2 events in the signal region at 2ns $\leq t^{\gamma}_{\rm corr} \leq$ 10 ns with 1.3±0.7 predicted.

Requirement	Expected Background				Expected Signal	Data
	SM	Beam Halo	Cosmics	Total	($m_{\tilde{\chi}} = 100$ GeV, $\tau_{\tilde{\chi}} = 5$ ns)	
Photon, $\not\!\!E_T$ and jet baseline cuts && 1.2ns $\leq t^{\gamma}_{\rm corr} \leq$ 10 ns	490.74±295.40	0.27±0.12	1.30±0.49	492.3±295.4	11.7±1.4	398
$\not\!\!E_T > 40$ GeV	162.96±76.19	0.24±0.12	1.17±0.46	164.4±76.2	10.2±1.2	99
Jet $E_T > 35$ GeV	154.52±72.96	0.12±0.08	0.79±0.37	155.4±73.0	9.4±1.1	97
$\Delta\phi(\not\!\!E_T, \text{jet}) > 1.0$	13.07±11.57	0.10±0.07	0.52±0.30	13.7±11.6	8.5±1.0	8
2ns $\leq t^{\gamma}_{\rm corr} \leq$ 10 ns	0.71±0.60	0.07±0.05	0.46±0.26	1.3±0.7	5.7±0.7	2

TABLE XI: Summary of the expected and observed number of events from the background estimate after each event selection requirement, separated for each background, and the expected number of signal events for a GMSB example point at $m_{\tilde{\chi}} = 100$ GeV/c^2 and $\tau_{\tilde{\chi}} = 5$ ns. Note that we apply the additional requirement $1.2 < t^{\gamma}_{\rm corr} < 10$ ns to allow the method to use the control regions to make predictions at each stage. The chosen set of requirements from the optimization is: Photon E_T >30 GeV, jet E_T >35 GeV, $\Delta\phi(\not\!\!E_T, \text{jet})$ >1.0, $\not\!\!E_T$ >40 GeV, 2ns $\leq t^{\gamma}_{\rm corr} \leq$ 10 ns. The baseline cuts include all cuts in Tables III and IV. The background predictions match well with the observed number of events for each requirement indicating the background estimation methods are reliable. There is no evidence of new physics

Preselection Requirements	
$E_{\rm T}^{\gamma} > 30$ GeV, $\not\!\!E_T > 30$ GeV	54
Photon ID and Fiducial, $\lvert\eta\rvert < 1.0$	39
Good Vertex, $\sum_{\rm tracks} p_T > 15$ GeV/c	31
$\lvert\eta_{\rm detector}^{\rm jet\ cone\ 0.7}\rvert < 2.0$, $E_{\rm T}^{\rm jet} > 30$ GeV	24
Cosmic Rejection: $\Delta\phi(\mu{-}{\rm stub}, \gamma) > 30^{\circ}$	23
Requirements after Optimization	
$\not\!\!E_T > 40$ GeV, $E_{\rm T}^{\rm jet} > 35$ GeV	21
$\Delta\phi(\not\!\!E_T, {\rm jet}) > 1$ rad	18
2.0 ns $< t_{\rm corrected}^{\gamma} <$ 10 ns	6

TABLE XII: The expected acceptance for a GMSB example point at $m_{\tilde{\chi}} = 100$ GeV/c^2 and $\tau_{\tilde{\chi}} = 5$ ns after the event selection requirements, shown for completeness as it is presented in the PRL.

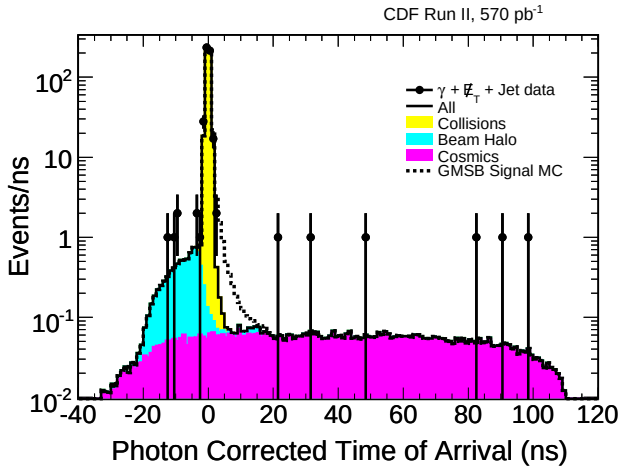

(a)

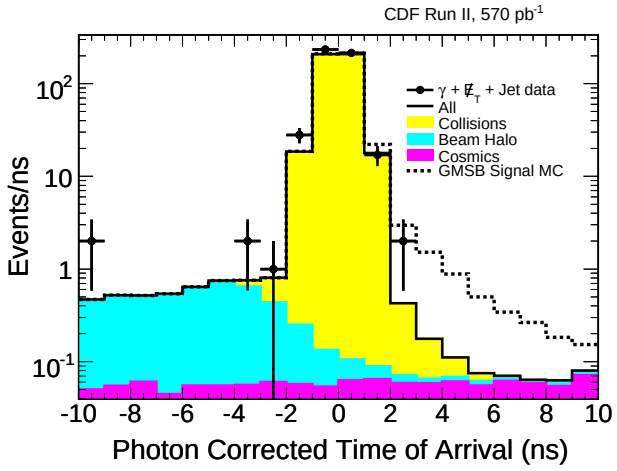

(b)

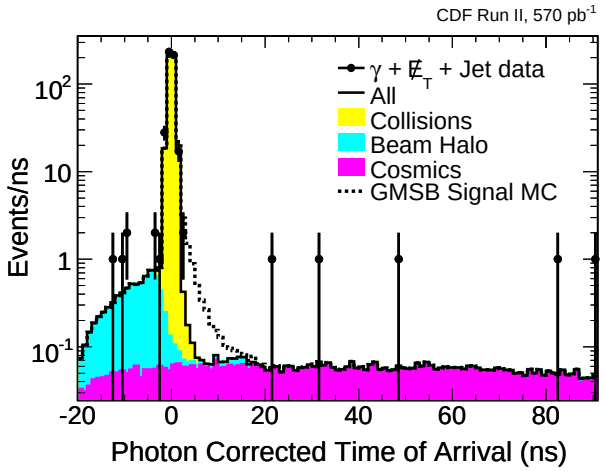

(c)

FIG. 9: The $t^{\gamma}_{\rm corr}$ distribution after all but the timing cut for all backgrounds, the expected signal and the observed data. We count 508 events in the full time window (a) and expect 6.2±3.5 from cosmics and 6.8±4.9 from beam halo and the rest from SM. We observe 2 events in the signal region at $2 < t^{\gamma}_{\rm corr} < 10$ ns (b) consistent with the background expectation of 1.3±0.7 events. Table XI lists the expected number of events for the various sources. Figure (c) is added for completeness as it is presented in the PRL.

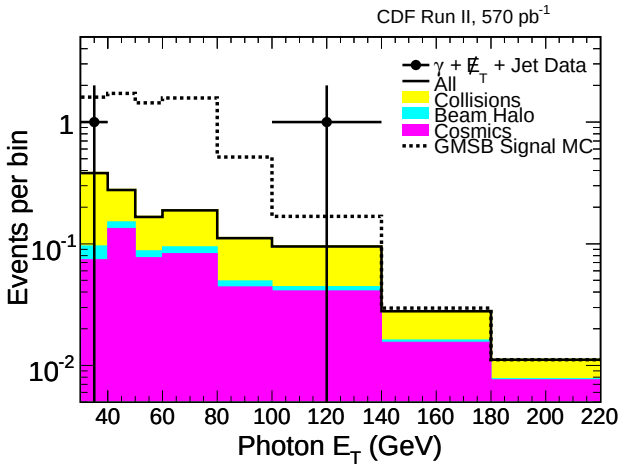

(a)

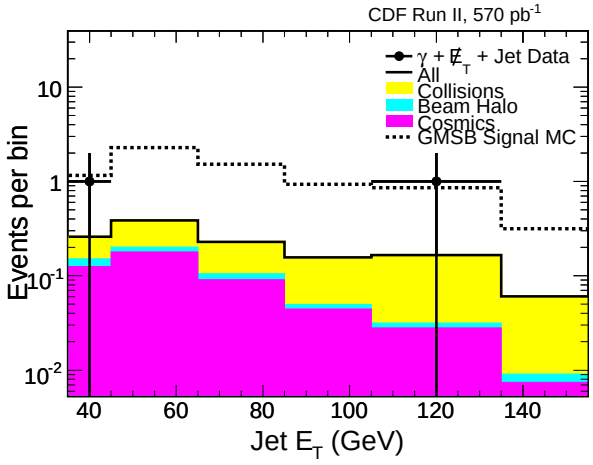

(b)

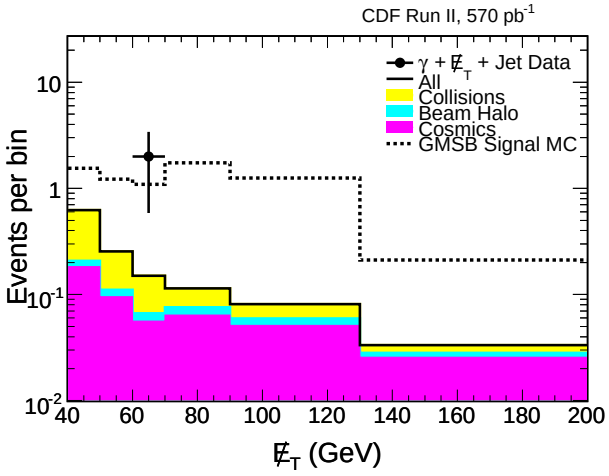

(c)

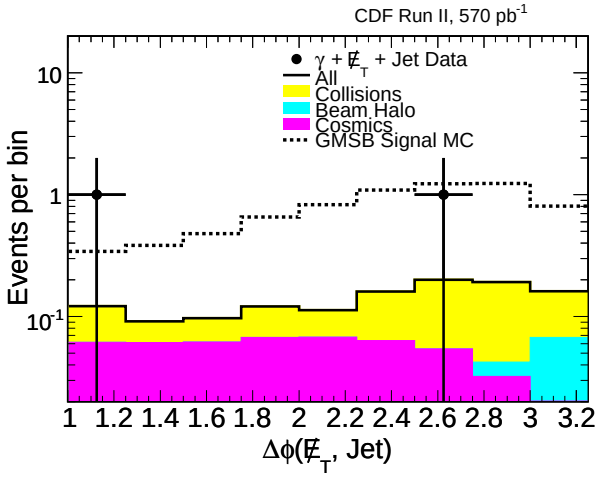

(d)

FIG. 10: The same as Fig. 7, but including the data in the signal region. Each variable is plotted down to their optimized requirement value. There is no evidence for new physics.

B. Parametrization of the Efficiency · Acceptance

In order to get smooth exclusion regions and set model independent limits, we parameterize our acceptance as a function of both $\widetilde{\chi}_1^0$ mass and lifetime using a fit to the efficiency · acceptance of the simulated GMSB points. There are several effects that are both a function of the $\widetilde{\chi}_1^0$ mass and lifetime. An event has to contain at least one photon that passes the selection criteria, hence at least one $\widetilde{\chi}_1^0$ has to decay in the detector [6]. Similarly, in order to pass the timing requirement, the $\widetilde{\chi}_1^0$ has to decay within a timing window. The probability of these effects to happen as a function of lifetime determine the functional form of the acceptance, $P_{\rm vol}$, and the efficiency, $P_{\rm t}$, respectively. After a fit to the results in Table IX we take:

$$P_{\rm t} = (-0.0449877 + 8.69673 \cdot 10^{-3} m_{\tilde{\chi}} - 3.49779 \cdot 10^{-5} m_{\tilde{\chi}}^2) \cdot (1 - (1 - e^{-4.78942/(\tau_{\tilde{\chi}}+1.21742)})^2) \quad (4)$$

and

$$P_{\rm vol} = (-0.254525 + 6.85926 \cdot 10^{-3} m_{\tilde{\chi}} - 1.54730 \cdot 10^{-5} m_{\tilde{\chi}}^2) \cdot (1 - e^{-(-0.625378+0.0647422 \cdot m_{\tilde{\chi}})/(\tau_{\tilde{\chi}}+0.842287)}) \quad (5)$$

Each of these functions consists of two multiplicative terms: a mass-dependent term that determines the overall scale and a lifetime dependent term that has the functional form of the probability distributions described above. The additive term in the denominator of the exponential is needed as at low $\widetilde{\chi}_1^0$ lifetimes both acceptance and efficiency are not zero and are dominated by the finite resolution of the timing measurement. The slight mass-dependence in the second term of $P_{\rm vol}$ comes from the momentum variation with mass which makes the $\widetilde{\chi}_1^0$ leave the detector faster/slower [6]. All numbers are determined from fits to the 2-dimensional distribution of simulated GMSB points as a function of $\widetilde{\chi}_1^0$ mass and lifetime. With these functions we get an accuracy of ∼10%, where we define accuracy as the relative difference between the values of the fit-function and the simulated GMSB points. To further improve the accuracy such that it is well below the systematic uncertainty in Section VI we introduce a function, $P_{\rm corr}$, that is not further motivated to take care of the deviations:

$$P_{\rm corr} = 1.04 - \frac{0.2}{55.0}\tau_{\tilde{\chi}} - \frac{0.011}{0.06 + (1 - \tau_{\tilde{\chi}})^2} \quad (6)$$

A comparison of the parameterization with the results in Table IX is shown in Figure 11. Subfigure (a) shows that the accuracy of the fit is ∼4%, well below the systematic uncertainty (see Table VII). Hence we will neglect this uncertainty when we show the exclusion regions. Figs. (b) and (c) show that there is no tendency as a function of $\widetilde{\chi}_1^0$ lifetime and mass. Figure 12 shows examples of the fits for $\widetilde{\chi}_1^0$ masses of 67, 80, 94 and 113 GeV/c^2. In the next section we show the exclusion regions.

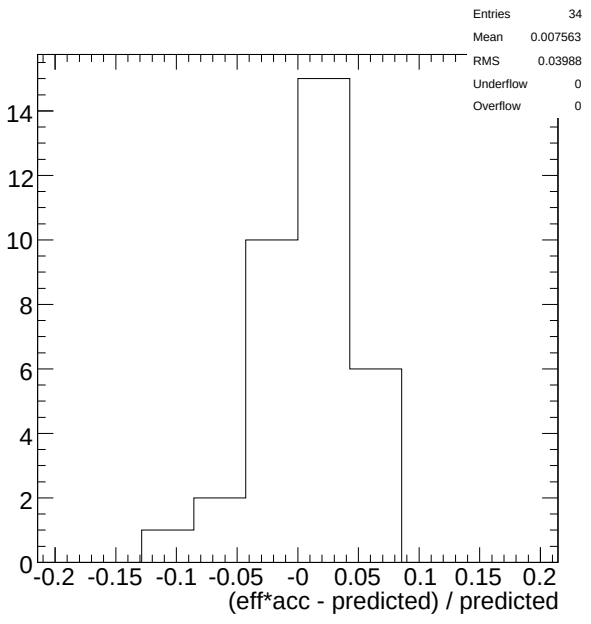

(a)

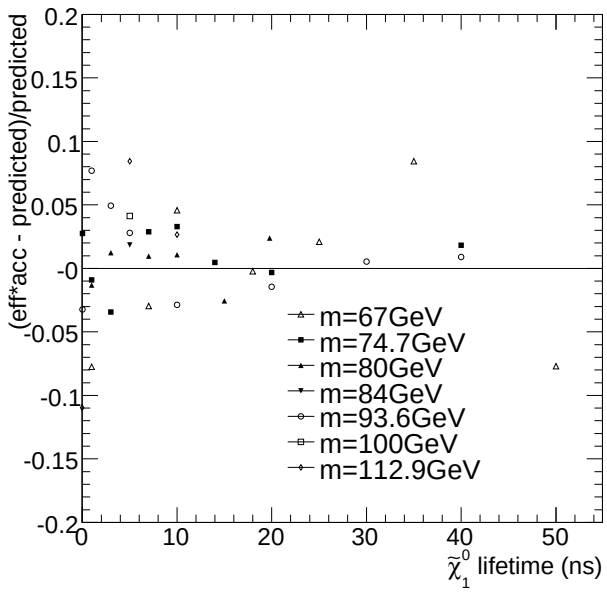

(b)

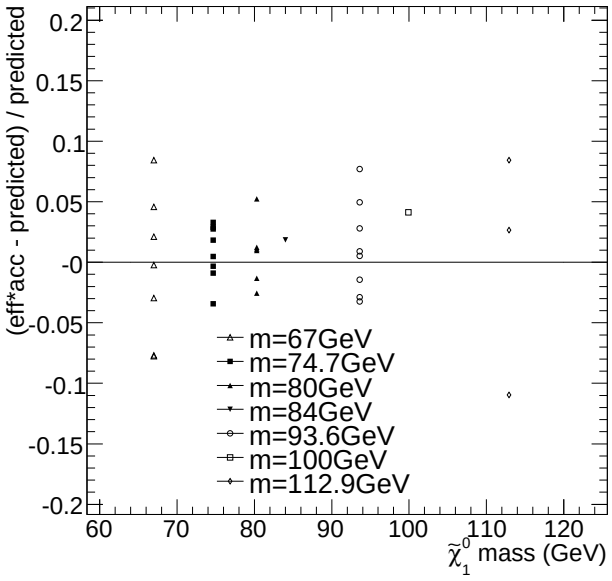

(c)

FIG. 11: The quality of the efficiency·acceptance model that we use to interpolate the simulated points for the cross section limits and the exclusion region. This is shown as the relative difference between the model and the simulated GMSB acceptance points in (a). The overall RMS is $\sim 4\%$, well below the systematic uncertainty. Figures (b) and (c) show the relative difference as a function of $\widetilde{\chi}_1^0$ lifetime and mass. There is no tendency towards lifetime or mass observed.

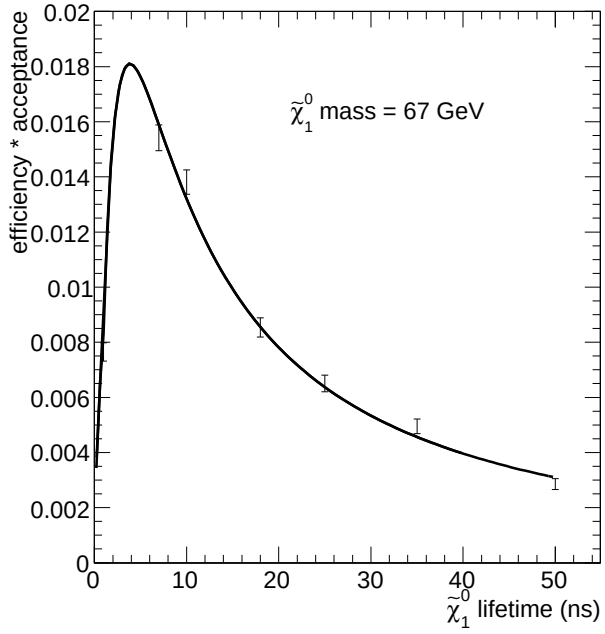

(a)

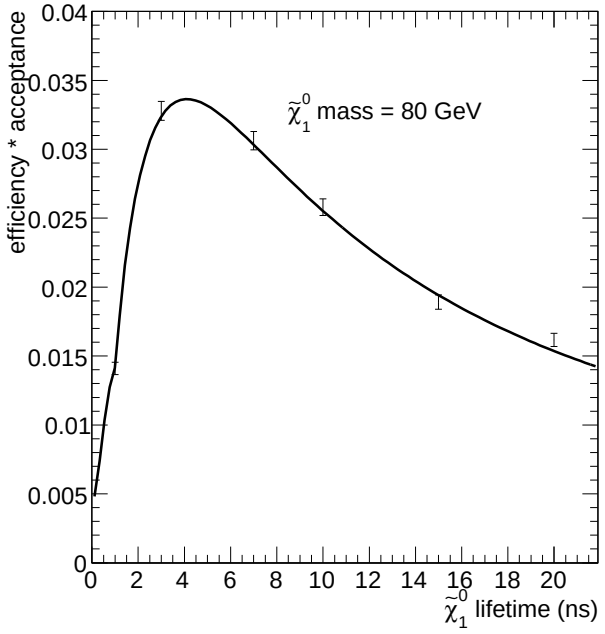

(b)

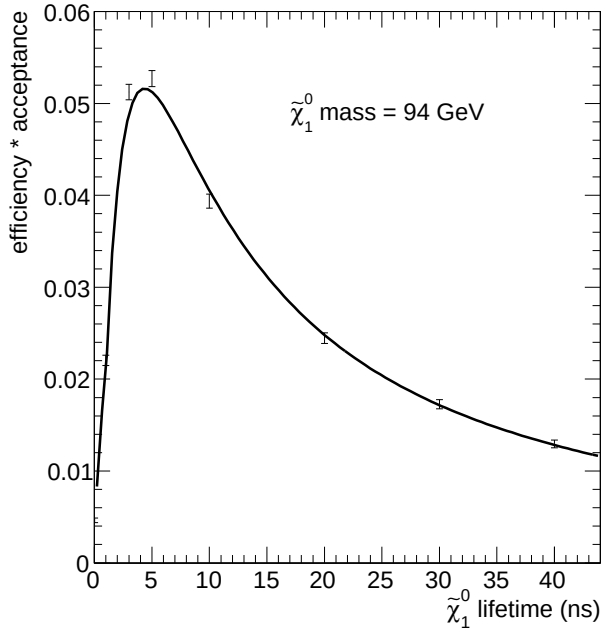

(c)

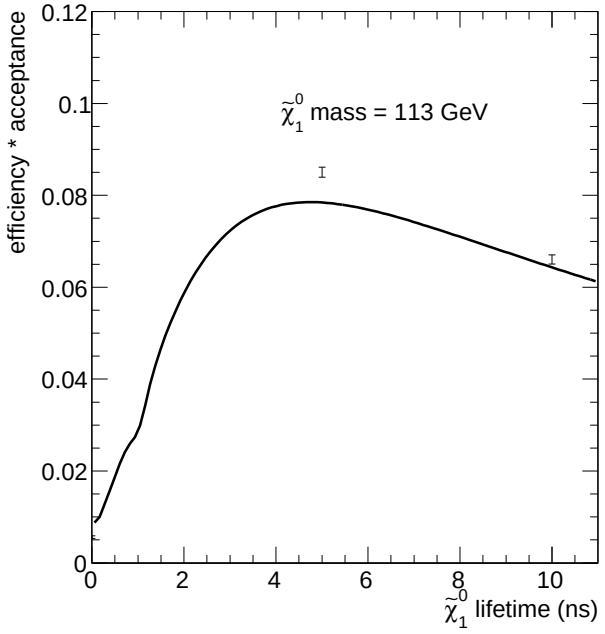

(d)

FIG. 12: Fits and MC points of the eff·acc vs. lifetime for masses 67 GeV/c^2 (a), 80 GeV/c^2 (b), 94 GeV/c^2 (c) and 113 GeV/c^2 (d). As in Fig. 11 the acceptance is well modeled by our parameterization.

C. Model-independent Cross Section Limits and GMSB Exclusion Regions

Figure 13 shows the predicted and observed cross section limits along with the NLO production cross section as a function of $\widetilde{\chi}_1^0$ lifetime at a mass of 100 GeV/c^2 and as a function of mass at a lifetime of 5 ns. Indicated in green is the 6.5% uncertainty-band on the production cross section (see Table VII). In yellow we show the expected variation in the expected cross section limit (∼30%) using the data in Table XIII and the RMS definition in Eq. 3. We reach the highest sensitivity at a lifetime of ∼5 ns as the limit follows the shape of the eff·acc curves shown in Fig. 12. We have no sensitivity at lifetimes less than ∼1 ns as few of the $\widetilde{\chi}_1^0$ have long lifetimes and consequently do not produce delayed photons. However, most of the parameter space there should already be excluded by searches in $\gamma\gamma + \not\!\!E_T$ [5]. We lose sensitivity as a function of mass as the production cross section decreases rapidly. Taking into account all simulated points, interpolated using the function shown in the previous section, we show the contours of constant cross section limit for the observed number of events in Fig. 14a. This figure shows (a) that for any mass we are most sensitive to lifetimes of ∼5 ns, and (b) that we lose sensitivity as either the mass or the lifetime increases. Since the kinematics of GMSB are probably typical for models that produce delayed $\gamma + \not\!\!E_T + \geq 1$ jet events it allows for a sensitivity estimate to any proposed signal model other than GMSB, by comparing the shown expected cross section limit to the proposed production cross section. Finally, Fig. 14b shows the 95% C.L. NLO exclusion region using the fixed choice of cuts from the optimization both for the predicted and observed number of background events. The $\widetilde{\chi}_1^0$ mass reach, based on the predicted (observed) number of events is 108 GeV/c^2 (101 GeV/c^2), at a lifetime of 5 ns. The predicted (observed) lifetime reach is 25 ns (21 ns) at the lowest simulated mass of 67 GeV.

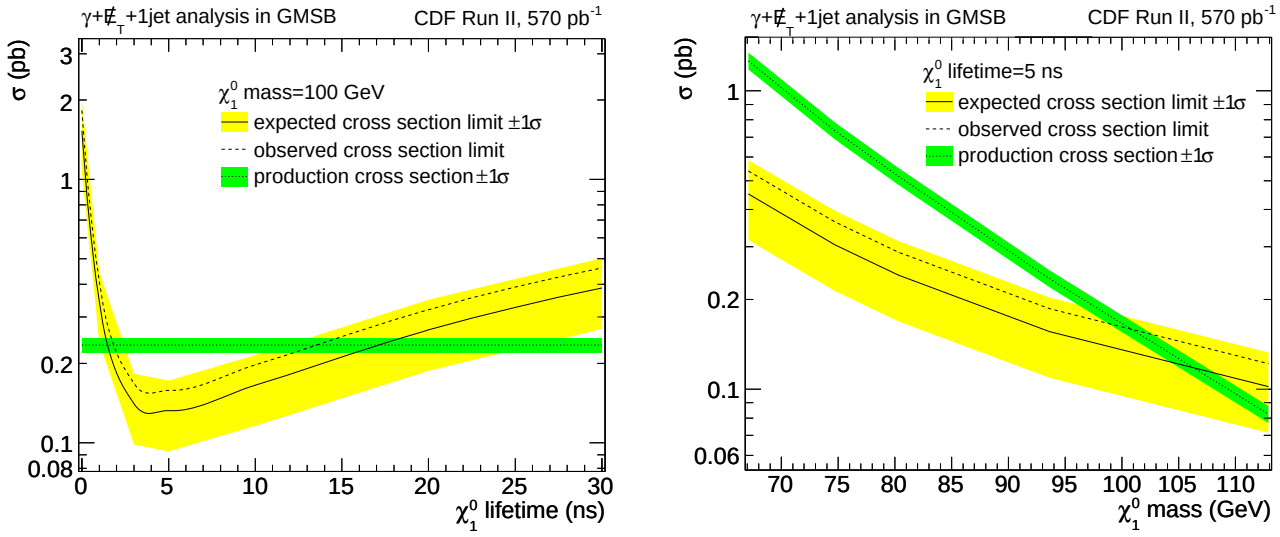

(a) (b)

FIG. 13: The predicted and observed cross section limits as a function of the $\widetilde{\chi}_1^0$ lifetime at a mass of 100 GeV/c^2 (a) and as a function of the $\widetilde{\chi}_1^0$ mass at a lifetime of 5 ns (b). Indicated in green is the 6.5% uncertainty-band for the production cross section (see Table VII), in yellow the statistical uncertainty of the background prediction on the cross section limit (∼30%).

N_{obs}	$\sigma_{\rm obs}(N)$ (pb)	Probability
0	0.0799	0.287
1	0.120	0.358
2	0.153	0.224
3	0.196	0.0932
4	0.239	0.0291
5	0.280	0.00729

TABLE XIII: The expected 95% C.L. cross section limit as a function of the hypothetically observed number of events and the Poisson probability for this number of events. The expected limit and its variation are calculated as shown in [30] with Eqs. 2 and 3 using the optimized background expectation, acceptance and production cross section at an example GMSB point of $m_{\tilde{\chi}}$ =100 GeV/c^2 and $\tau_{\tilde{\chi}}$ =5 ns. With these numbers we get an expected cross section limit of 128 fb and an RMS on the limit of 42 fb, or ∼30%.

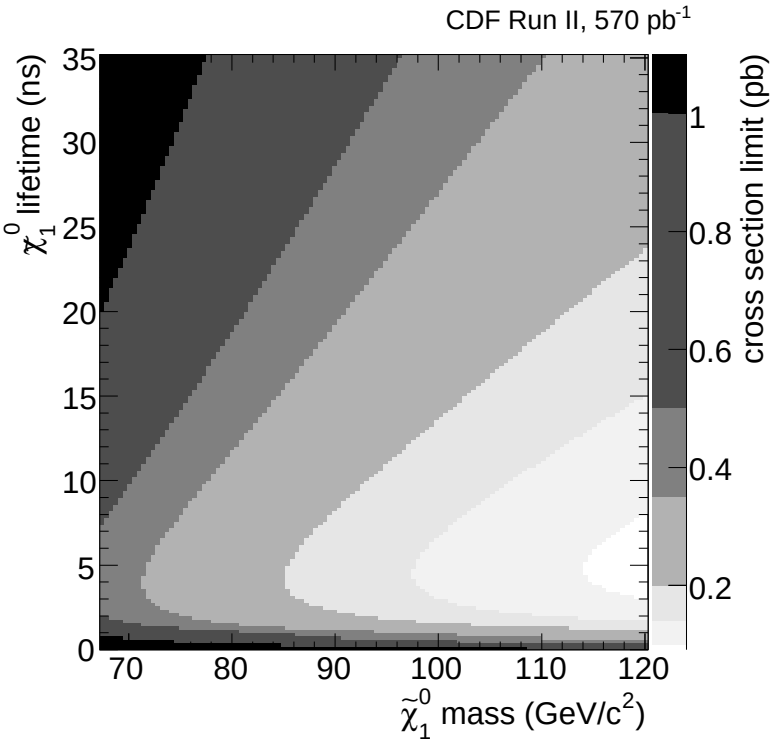

(a)

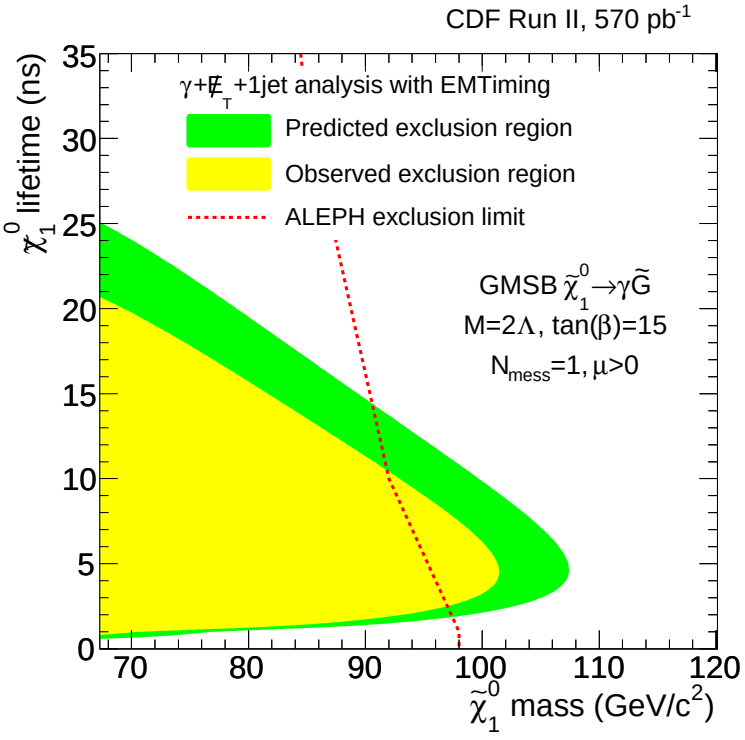

(b)

FIG. 14: In (a) the contours of constant cross section limit, using the eff·acc interpolation, for the observed number of events. The visible contours are: {0.1, 0.2, 0.35, 0.5, 1.0} pb. In (b) the predicted and observed exclusion region using the interpolation function, along with the limit from ALEPH/LEP [5]. We have the highest mass reach of 108 GeV/c^2 (predicted) and 101 GeV/c^2 (observed) at a lifetime of 5 ns.

IX. CONCLUSIONS

We have presented the results of a search for heavy, neutral, long-lived particles that decay to photons in a sample of $\gamma + \not\!\!E_T + \geq 1$ jet events. Candidate events were selected based on the delayed arrival time of the photon at the calorimeter as measured with the EMTiming system. We found 2 events using 570 pb^{-1} of data in run II which is consistent with the background estimate of 1.3±0.7 events. Using a gauge mediated supersymmetry breaking model with $\widetilde{\chi}_1^0 \rightarrow \gamma\widetilde{G}$ we set quasi model-independent cross section limits, as well as find the exclusion region in the $\widetilde{\chi}_1^0$ lifetime vs. mass plane with a mass reach of 101 GeV/c^2 at $\tau_{\tilde{\chi}} \simeq 5$ ns. Our results extend the world sensitivity to these models beyond those from LEP II.

To investigate the prospects of a search at higher luminosity we calculate the cross section limit assuming all backgrounds scale linearly with luminosity while their uncertainty fractions remain constant. The resulting background and cross section limit improvement along with the N_{95} are shown in Table XIV for a GMSB example point at $m_{\tilde{\chi}} = 100$ GeV/c^2 and $\tau_{\tilde{\chi}} = 5$ ns. Figure 15 shows the predicted exclusion region for a luminosity of 2 and 10 fb^{-1}. The Figure suggests a further expansion of the exclusion region far beyond the LEP limits.

Luminosity (fb^{-1})	Background	N_{95}	Factor of $\sigma_{\rm exp}$ Improvement
0.570	1.3±0.7	4.60	1
2	4.3±2.3	7.44	0.46
10	21.9±11.6	24.8	0.309

TABLE XIV: The expected improvement for various luminosities for a GMSB example point at $m_{\tilde{\chi}} = 100$ GeV/c^2 and $\tau_{\tilde{\chi}} = 5$ ns assuming all backgrounds scale linearly with luminosity while their uncertainty fractions remain constant. The resulting exclusion region is plotted in Fig. 15.

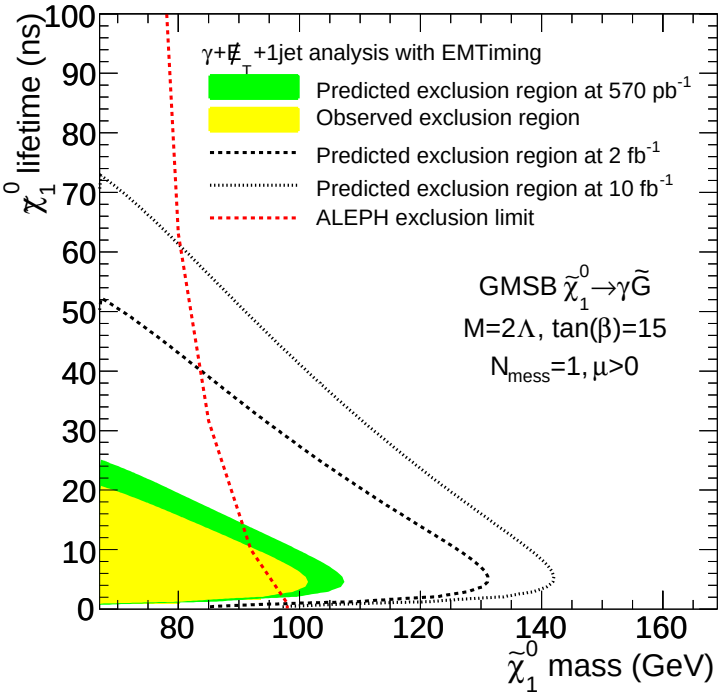

FIG. 15: The dashed lines show the prediction of the exclusion limit after a scaling of the background prediction and the uncertainties for a luminosity of 2 fb^{-1} and 10 fb^{-1} respectively.

Acknowledgments

The authors would like to thank Ray Culbertson, Bob Blair, Henry Frisch, Franco Bedeschi, Alexandre Pronko and Soon Jun for helpful advice and support of this analysis.

---

[1] M. Goncharov *et al.*, "The Timing System for the CDF Electromagnetic Calorimeters," CDF Note 7918 (2005), NIM A**565**, 543 (2006).
[2] http://hepr8.physics.tamu.edu/hep/emtiming/
[3] See for example S. Ambrosanio, G. L. Kane, G. D. Kribs, S. P. Martin and S. Mrenna, Phys. Rev. D **54**, 5395 (1996) or C. H. Chen and J. F. Gunion, Phys. Rev. D **58**, 075005 (1998).
[4] CDF Collaboration, F. Abe *et al.*, Phys. Rev. D **59** 092002 (1999).
[5] ALEPH Collaboration, A. Heister *et al.*, Eur. Phys. J. C **25**, 339 (2002); also see L3 Collaboration, arXiv:hep-ex/0611010; OPAL Collaboration, Proc. Sci. HEP2005 346 (2006); DELPHI Collaboration, Eur. Phys. J. C **38** 395 (2005).
[6] P. Wagner and D. Toback, Phys. Rev. D **70**, 114032 (2004).
[7] There are unpublished limits by other LEP collaborations on GMSB models but not as stringent as by ALEPH. See for example the papers at http://lepsusy.web.cern.ch/lepsusy/www/photons/single/ single_public_summer04.html and the talk at http://susy06.physics.uci.edu/talks/1/gataullin.pdf
[8] CDF Collaboration, "Search for Heavy, Long-Lived Particles that Decay to Photons at CDF," public CDF Note 8378 (2006).
[9] M. Goncharov, V. Krutelyov, D. Toback and P. Wagner, "Methods for Determining the Photon Timing Distributions for Searches with Final State Photons," CDF Note 7960 (2005).
[10] M. Goncharov, V. Krutelyov, D. Toback and P. Wagner, "Space-Time Vertex Reconstruction Using COT Tracks," CDF Note 8015 (2005).
[11] M. Goncharov, V. Krutelyov, D. Toback and P. Wagner, "Resolution and Simulation of the EMTiming System," CDF Note 7928 (2006).
[12] M. Goncharov, D. Toback and P. Wagner, "Identification Efficiencies for Photons from Heavy, Long-Lived, Neutral Particles," CDF Note 7929 (2006).
[13] M. Goncharov, V. Khotilovich, V. Krutelyov, S.W. Lee, D. Toback and P. Wagner, "Performance of the EMTiming System as Seen by the ObjectMon Online Monitoring System," CDF Note 7515.
[14] We follow B. C. Allanach *et al.*, Eur. Phys. J. C **25**, 113 (2002), and take the messenger mass scale $M_{\rm M} = 2\Lambda$, $\tan(\beta) = 15$, $\mathrm{sgn}(\mu) = 1$ and the number of messenger fields $N_{\rm M} = 1$. The parameters $c_{\rm Grav}$ (gravitino mass factor) and Λ (supersymmetry breaking scale) are allowed to vary.
[15] The remaining processes produce slepton pairs that also decay to pairs of $\widetilde{\chi}_1^0$: τ_1 ($\sim 9\%$), e_R ($\sim 7\%$), μ_R ($\sim 7\%$).
[16] CDF Collaboration, D. Acosta *et al.*, Phys. Rev. D **71** 031104 (2005).
[17] W. Beenakker *et al.*, Phys. Rev. Lett. **83**, 3780 (1999).
[18] P. Simeon and D. Toback, "An Advantage of Setting Cross Section Limits on the Total Production Mechanism When Multiple Processes Produce the Same Final State," CDF Note 7084 (2006).
[19] http://www-cdf.fnal.gov/internal/physics/top/jets/systematics.html
[20] http://www-cdf.fnal.gov/internal/physics/joint_physics/agenda/20050527-minutes.html
[21] O. Gonzalez and C. Rott, "Uncertainties due to the PDFs for the gluino-sbottom search," CDF Note 7051 (2005).
[22] M. Griffiths *et al.*, "Searches for Chargino and Neutralino in the e+e/mu+e/mu with 1 fb-1 of data," CDF Note 8389 (2006).
[23] see e.g. W. Beenakker *et al.*, Nucl. phys. B **492**, 51 (1997); Prospino 2.0: http://www.ph.ed.ac.uk/∼tplehn/prospino/prospino.html
[24] P. Onyisi, "Run 2 gamma+met search," CDF Note 6381 (2003).
[25] http://www-cdf.fnal.gov/internal/physics/photon/docs/cuts.html
[26] We note that this number is different from the 14% described in Ref. [9]. This should be understood because the fraction is only based on the probability that the highest-$\Sigma p_{\rm T}$ vertex in the event is the same vertex that produces the photon. For instance, as $Z\gamma \to \nu\nu\gamma$ produces very few tracks in association with the photon so there is a low probability that the highest-$\Sigma p_{\rm T}$ vertex produces the photon at high luminosity. As a second example, in $t\bar{t}\gamma \to \gamma +$ jets events the photon is very likely to come from the highest-$\Sigma p_{\rm T}$ vertex.
[27] PYTHIA: T. Sjöstrand, L. Lönnblad and S. Mrenna, arXiv:hep-ph/0108264 (2001); *cdfsoft* 6.1.2 has PYTHIA version 6.216. *cdfSim*: G.S. Sganos, Tutorial on cdfSim. We modified it for the simulation of the EMTiming system [11]. It further includes a bug-fix of the tracking code to simulate the CES response to photons from displaced vertices correctly and a patch by A. Scott to include decay products of displaced $\widetilde{\chi}_1^0$ in the detector simulation [12].
[28] The ISASUGRA output is converted to PYTHIA using a script by A. Scott.
[29] R. Rossin, CDF Detector Lectures: "Systematics on the Luminosity Measurement," http://fcdfwww.fnal.gov/internal/WebTalks/Archive/0410/041007_clclum_detector_lecture/04_041007_clclum_detector_lecture_Roberto_Rossin_1_RobertoCLC_detector-04-10-07.pdf; S. Klimenko, J. Konigsberg and T. M. Liss, FERMILAB-FN-0741 (2003).

[30] E. Boos, A. Vologdin, D. Toback and J. Gaspard, Phys. Rev. D **66**, 013011 (2002). J. Conway, CERN Yellow Book Report No. CERN 2000-005 (2000), p. 247.